Materials Science and Engineering Laboratory

Nanometrology: FY 2003 Program and Selected Accomplishments

MSEL

Clare Allocca
Senior Scientific Advisor to the Director, MSEL

Stephen Freiman
Deputy Director, MSEL

Table of Contents

Nanometrology Program

The emphasis on nanotechnology around the world is leading to the development and commercialization of unique products based upon significantly smaller devices and material ensembles. Materials at the nanoscale in three dimensions (NEMS, MEMS), two dimensions (ultrathin films), and one dimension (carbon nanotubes) are growing in importance. Within the next few years novel devices at the micro- and nanoscale are expected to play key roles in a spectrum of industry sectors, including manufacturing, information technology, electronics, and healthcare. Nanometrology, *i.e.*, the measurement of dimensions, characterization of materials, and elucidation of structures of new and novel materials at the nanoscale, will be critical to the commercial development of this exciting new field.

The objective of the MSEL Nanotechnology Program is the development of metrology at the nanoscale for bulk and surface material properties as well as process monitoring. The Program encompasses metals, ceramics, and polymers in various forms — particles, thin films, nanotubes, and self-assembled structures. The Program is divided into five categories: **Nanomechanics**, **Nanocharacterization**, **Nanoelectronics**, **Nanomagnetics**, and **Nanomanufacturing**. This report contains short descriptions of selected accomplishments in these five areas.

A primary focus of **nanomechanics** is the measurement and understanding of mechanical properties of materials at the nanoscale, as well as prediction of nanomechanical properties based upon those in bulk materials. As one example, four methods for the determination of the elastic properties of thin films — atomic force acoustic microscopy, surface acoustic wave spectroscopy, Brillouin light scattering, and nanoindentation — are being compared using common sets of specimens. This study should lead to a better understanding of the complementary nature of these techniques for measuring a fundamental property of nanostructured materials and their combined use to determine supplementary properties such as film thickness or density. Reference materials for use in nanoindentation are being developed in collaboration with other National Measurement Institutes. Another aspect of mechanical properties at the nanoscale is that of nanotribology, the study of nanoscale friction and wear. Friction and stiction have been identified as key issues in the implementation of new devices based upon nanoelectromechanical technology, *i.e.*, NEMS. Recent work has involved the study of lubrication of magnetic hard discs.

One of the projects in **nanoelectronics** involves the quantitative determination of nanometer-size pore distributions in low dielectric constant films using small angle neutron scattering. This work has revealed subtle material characteristics hitherto unrecognized

by other techniques. A second project encompasses the development of models and the accompanying verification of advanced metallization techniques for sub-100 nm electronics. This work is focused on the development of processes for superfill of fine features in electronic devices and extends already developed models for such mechanisms. Finally, small angle x-ray scattering is being employed to measure the critical dimensions in pattern sizes for the semiconductor industry.

In the broad area of **nanocharacterization**, a number of topics are under investigation. New measurement procedures and reference materials for determining size distributions for nanoparticles (< 500 nm) are being addressed. Another exciting area of nanotechnology is the use of carbon nanotubes in ultra-stiff and strong composites, as electronic components, and as probes for use in scanned probe microscopy. During this past year, MSEL, in partnership with NASA and other NIST Laboratories, held a workshop whose goal was to identify the crucial measurement issues with respect to purity and dispersion of carbon nanotubes. Measurement protocols and conclusions emerging from this workshop will be published in the *Journal of Nanoscience and Nanotechnology*. A second such workshop is being planned for September of 2004.

MSEL has considerable experience in the measurement of parameters critical to **nanomagnetics**. For example, the shift to perpendicular magnetic recording presents issues in the dynamics, damping, and defects in recording media. MSEL is conducting modeling and measurements of ferromagnetic resonance on these materials. Work is also being carried out in the determination of the magnetic properties of nanostructured materials using a magneto-optic indicator film technique.

As an aid to carrying out **nanomanufacturing** processes, measurement procedures are being developed to measure flow properties of fluids at the nanoscale. Also, sensors are being investigated that can be used to monitor processing of polymer-clay nanocomposites.

Finally, MSEL supports several unique measurement instruments including the NIST Center for Neutron Research, and synchrotron x-ray beamlines at both the National Synchrotron Light Source at the Brookhaven National Laboratory and the Advanced Photon Source at the Argonne National Laboratory. Each of the facilities has developed instrumentation to be able to measure features of nanometer dimensions. In addition, combinatorial materials synthesis procedures are being addressed as part of a multiclient consortium. Details of this consortium can be accessed at **www.nist.gov/combi**.

Metrology for Nanoscale Properties: Nanoscale Mechanical Properties

We are developing AFM-based techniques to measure nanoscale mechanical properties in situ. Atomic force acoustic microscopy enables quantitative point measurements of elastic modulus as well as images of relative stiffness. The information obtained furthers our understanding of the nanomechanical properties of surfaces and thin-film structures.

Donna Hurley

The accelerating race towards the nanoscale presents a serious challenge for materials characterization. Tools that can assess properties with submicrometer spatial resolution must be developed. Specifically, the need exists for nanoscale mechanical-property information. Knowledge of properties like elastic modulus or stiffness and interfacial quality (defects, adhesion, strain) is critical to successful development of new film materials and nanoscale assemblies. Likewise, such information could help assess integrity or reliability in applications ranging from microelectronics to biotechnology.

To fill this need, we are developing tools that exploit the spatial resolution of atomic force microscopy (AFM). Our approach, called atomic force acoustic microscopy, (AFAM), involves exciting mechanical resonances of the AFM cantilever when in contact with a sample. By comparing spectra for the unknown (test) material and a reference sample with known properties, the indentation modulus M can be measured. The small tip diameter ($\sim 20{-}100$ nm) means that we can obtain *in situ* elastic stiffness images with nanoscale spatial resolution.

In FY03, we continued developing AFAM techniques for quantitative measurements. We examined a thin Nb film with two reference samples and two cantilevers. Two analysis methods were used: an analytical model for the dynamics of a uniform rectangular beam, and a finite element method (FEM) that allowed for a variable cantilever cross-section. By averaging the results from both reference materials, values for M were in very good agreement (5 % different) with those obtained by SAW spectroscopy and nanoindentation. For a cantilever that approximated a rectangular beam, the analysis methods yielded very similar values for M. For cantilevers with a nonuniform cross-section, viscoelastic damping had to be included in the FEM analysis. Results from the two cantilevers were equal within measurement uncertainty.

We also examined a hydrogenated silicon carbide film using two reference samples. Values for M with either reference material alone were the same ($M = 70 \pm 3$ GPa)

within measurement uncertainty as those obtained from SAW spectroscopy and nanoindentation. From these results and those on the Nb film, we concluded that AFAM results are more accurate when the modulus ratio $M_{test}/M_{reference}$ is $\sim 0.9{-}1.1$. We are closely scrutinizing the measurement approach and its contact mechanics to better understand this requirement. Nonetheless, these results demonstrate our ability to reliably and accurately measure elastic properties at the nanoscale.
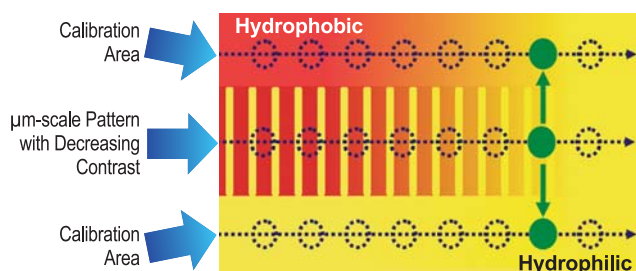
Figure 1: *Specimen for AFAM RH studies. Circles indicate data points along a line scan. Green areas show how minimum contrast to RH sensitivity is determined. (M. Fasolka, NIST)*

Potential relative humidity (RH) effects on AFAM measurements were revealed in experiments on a film of fluorinated silica glass. Values for M correlated roughly with outside RH and increased as the RH increased. We believe that the contact stiffness measurements were affected by a variable water layer between the tip and sample. We are working on laboratory RH control in order to investigate the effect systematically. Samples for these experiments, obtained in a collaboration with Polymers Division, will contain controlled variations in moisture sensitivity as shown in Figure 1. To interpret the experimental results, we are refining our data analysis models to include the effects of the water layer.

The work described above involved measurements of the flexural resonances of the AFM cantilever only. In upcoming months, we will extend our AFAM methods to examine torsional resonances as well. This information will allow us to investigate other nanoscale mechanical properties such as Poisson's ratio or friction.

Contributors and Collaborators

P. Rice (Materials Reliability Division, NIST); A. Kos (Magnetics Division, NIST); M. Fasolka, P. McGuiggan (Polymers Division, NIST); K. Shen, J. Turner (University of Nebraska); N. Jennett (NPL, UK); A. Rar, G. Pharr (University of Tennessee, ORNL); M. Kopycinska–Mueller, U. Rabe, W. Arnold (IZFP, Germany)

Nanoscale Measurement of the Amount of Complex Hydrocarbon Molecules on Magnetic Hard Disks

The requirement for protection in the head-disk interface is rising. In order to reach 1 Terabit/in² areal density and double the data transfer rate, the spacing between the head and disk is shrinking to 3.5 nm at a flying speed approaching 40 m/s. Occasional contacts will test the shear strength of the molecular layer on top of the carbon overcoat. Current lubricant molecules are alcohol-functionalized perfluoropolyether which are inert and oxidatively resistant but lack solubility and surface bonding strength. Alternative molecules such as multiply alkylated cyclopentanes are being considered to improve protection. In order for any alternate molecules to be used, the average molecular thickness on a hard disk surface needs to be measured accurately at 10Å ± 1Å. We have developed a unique master calibration technique that, for the first time, is able to accurately determine the average molecular thickness of a complex hydrocarbon mixture on magnetic hard disks.

Richard Gates, Charles Ying, and Stephen Hsu

The Information Storage Industry Consortium (INSIC) has set a goal of reaching 1Tbit/in² areal density by 2006 with a concurrent increase in data transfer rate approaching 100 Gbit/s. This translates to an extraordinarily ambitious technical goal of a 10-fold increase in capacity in four years. To reach that goal, the flight height and the carbon overcoat thickness need to be reduced to 3.5 nm and 1 nm respectively. Since the disk is protected by the thickness of the carbon overcoat and 10Å of lubricant molecules, alternative carbons and lubricant molecules are needed to provide the same degree of protection with one-fifth the amount of lubricant and overcoat.

Under the proposed new design, head-disk interface contacts are inevitable due to reduced flight height, waviness of the disk, and rotational wobble. One of the key characteristics that has been identified for protective molecules is the adhesive strength to resist high shearing action. A typical solution in this case would be to add strongly surface-bonding molecules to the lubricant as additives. The current disk lubricant, a functionalized perfluoroalkyl ether, has limited solubility. Therefore, hydrocarbon molecules with extremely low volatility characteristics are needed. Multiply alkylated cyclopentane is one such molecule.

Current industrial practice of measuring the thickness of perfluoroalkyl ether on a hard disk surface (tip to valley distance from 15 Å to 25 Å) relies on a cross calibration between fourier transform infrared spectroscopy (FTIR) and x-ray photoelectron spectroscopy (XPS) on CF2 bonds which is symmetrical and sharp. For complex hydrocarbons, there are multiple peaks interrelated at different frequencies, and there is no established technique for such measurement.

The measurement of "average film thickness" needs to be defined. The lubricant molecules are a complex mixture of isomers with different molecular weights. The surface is atomically rough, and the coverage is below the full "monolayer" level. Nano- and microscale aggregations undoubtedly take place, and the distribution of molecules across the surface hills and valleys is not known. Recent data from UC Davis tend to support this observation. High-frequency modulation atomic force microscopy (AFM) was used to image the surface, and from these data, elasticity information can be extracted. Figure 1 relates the topographic image with elasticity of a hydrocarbon covered hard disk surface. The bottoms of the valleys show higher hardness suggesting that the hydrocarbon molecules do not reside at the bottom of the valleys.
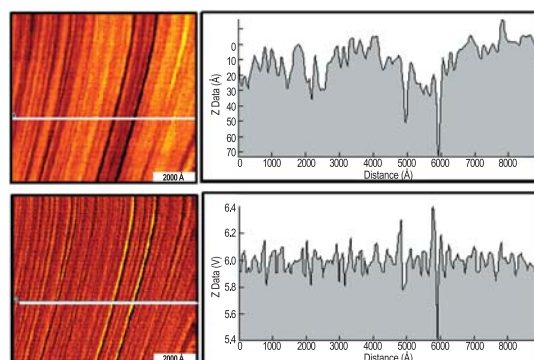
Figure 1: *AFM topographic images and elasticity data.*

Detection and measurement of a one nanometer thick complex molecular layer on a rough surface taxes the detection limits of analytical instrumentation. We first used FTIR and a modified XPS technique. The modified XPS technique scanned the surface twice: once without lubricant coverage and once with lubricant coverage. The decrease of x-ray photoelectron signal intensity from the molecule coverage was used to estimate film thickness. Unfortunately, the carbon overcoat thickness was found to vary along the radial direction of the disk. Depending on the specific batch of disks tested, the variation could be as much as 5 %–10 % from the inside radius to the outer edge of the disk. Hence, this measurement technique is insufficient to measure the "molecular thickness" as required by industry to control the process.

We tried various techniques such as AFM scratching, ellipsometry, and x-ray reflectivity (XRR). The latter technique has difficulty with surface roughness and the fact that the average film thickness is below the peak-to-valley distance. For AFM, the molecules wet the tip. Ellipsometry data at this range have large scatter. So the conclusion is there is no acceptable technique to measure such "film thickness" of a complex hydrocarbon molecular mixture to the industrial specification of 10 Å ± 1 Å.

To develop a solution to this industrially important issue, we created a master calibration sample approach. Basically we deposit a known (gravimetrically) solution on a disk with a barrier film surrounding a known area and allow the solvent to evaporate under controlled conditions. The resulting "film thickness" can then be used to calibrate various instruments. The challenges are uniform distribution of molecules across the area, containment of fluid, meniscus forces, and evaporation rate control.
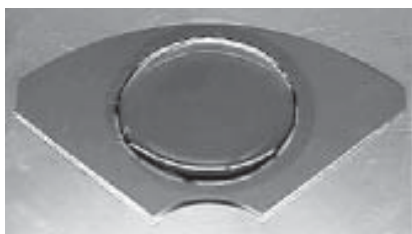
Figure 2: *Confined lubricant solution on a hard disk.*

Initially, this approach was attempted with liquid–phase samples; however, under these conditions, evaporation and meniscus forces lead to uncontrolled lubricant film uniformity. This was solved by evaporating the solvent from the mixture while it is in the solid state. The solution is placed within the barrier (Figure 2) and rapidly frozen using liquid nitrogen. Then the solvent is slowly removed by evaporation into an inert gas at –10 °C.

By controlled slow evaporation of solvent directly from a solid frozen state, we avoid the meniscus and surface tension forces which tend to create non-uniformity of the liquid mass. A pseudo "sublimation" process is created. In this way, uniform signal detection by FTIR confirms that the distribution of molecules across the area is less than 5 % at less than full monolayer coverage. Using this new technique, a series of "film thickness calibration standards" was created (see Figure 3).

A series of three master calibration samples was prepared and submitted for XPS photoelectron attenuation analysis. The very small variation of XPS intensity across the disk surface indicated that film uniformity was quite good, varying by less than 5 %. A correlation plot of XPS estimated thickness versus master calibration target thickness (Figure 4) yielded a

straight line, but the slope was not 1.0 (referenced in red). This indicates that the XPS attenuation technique has an inherent bias due to inaccurate assumptions in the model used in the analysis. The observation that the slope of the XPS versus target thickness correlation is 0.6 indicates that the initial XPS attenuation technique was underestimating the hydrocarbon film thickness by about 40 %. The effect has been attributed to the difference in density between the hydrocarbon and carbon overcoat. Utilizing this information, the model was refined to accommodate this effect.
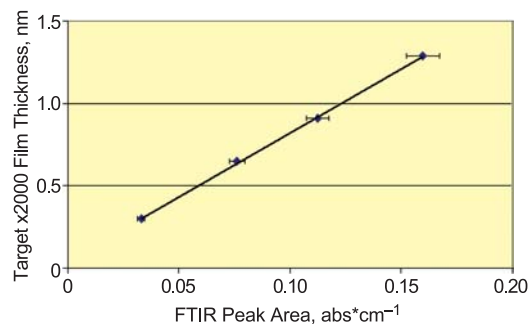
Figure 3: *Calibration curve relating FTIR signal to known hydrocarbon film thickness determined gravimetrically. Error bars are one standard deviation.*
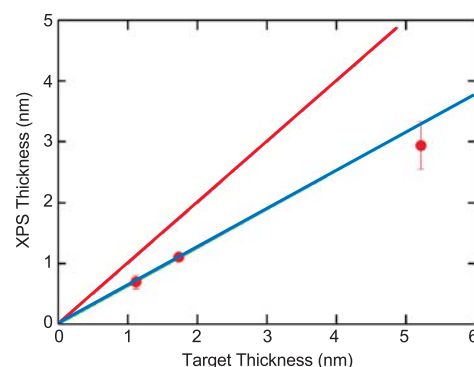
Figure 4: *XPS signal calibration for known hydrocarbon film thickness. Error bars are one standard deviation.*

A calibration method for nanometer-scale complex hydrocarbon films on an engineering surface has been developed. The method is based on gravimetric solution preparations and utilizes a novel freeze-evaporation technique to extract the carrier solvent while leaving a uniform film of complex hydrocarbon on the surface. The method can be applied to a variety of surfaces and offers the potential for calibrating many different analytical techniques for their ability to measure thickness of complex hydrocarbons.

For More Information on this Topic

S. Hsu (Ceramics Division, NIST)

Physical Properties of Thin Films and Nanostructures: Mechanical Properties of Thin Films

We develop and apply noncontact, nondestructive tools to measure thin-film mechanical properties such as elastic modulus and residual stress. Optical methods are used to determine the frequency dependence of the velocity of surface acoustic waves. The information obtained can assist in developing new film materials. It is also valuable for predicting the reliability and performance of thin-film components.

Donna Hurley and Vinod Tewary

Figure 1: *SEM micrograph of TiN film showing preferential crystallite orientation and adhesive Ti interlayer (R. Geiss, NIST).*

To successfully develop a new thin-film material, knowledge of its mechanical properties is often needed: to estimate surface residual stresses, to predict reliability or performance, or to assess film-substrate adhesion. Yet methods are generally limited to destructive tests or even "try it and see." Also, film properties usually cannot be extrapolated from those of bulk samples — if they exist.

We are developing nondestructive methods to quantify thin-film properties. We aim to relate physical properties like elastic moduli, residual stress, or adhesion to film microstructure, quality or performance. The approach exploits the behavior of surface acoustic waves (SAWs). The SAW velocity varies with frequency and depends on the film and substrate properties (Young's modulus E, Poisson ratio, density, and film thickness). We use laser ultrasonic methods to generate and detect SAWs over a broad frequency range. The SAW velocity-*versus*-frequency data are interpreted with a Green's function method to determine the film properties.

In FY03, we implemented a second SAW apparatus. Silicon and other materials are not opaque to infrared light and thus are ill-suited to the infrared detector in the original apparatus. The new apparatus uses a green laser in its interferometer, extending capabilities to a wider range of materials. In addition, a pulsed ultraviolet laser improves generation efficiency in polymer and other films. The apparatus is quite user-friendly, increasing accessibility to postdocs and visitors. This setup frees up our first apparatus for speculative experiments requiring more frequent reconfiguring of optical components.

Analysis capabilities were improved by extending the anisotropic Green's function inversion software to two layers. TiN films were analyzed with three different models: one elastically isotropic layer, one anisotropic layer, and two layers (isotropic TiN over hexagonal Ti). SEM images such as that in Figure 1 show a thin Ti interlayer, but, until now, we could not model two separate
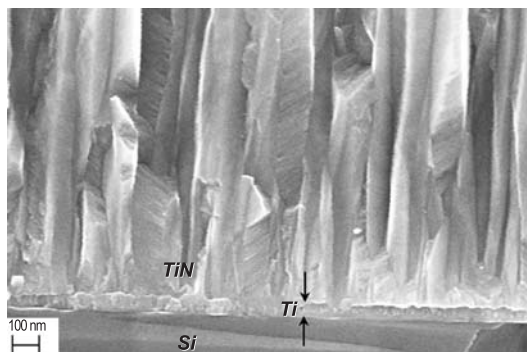
layers. Of the three models, the velocities predicted by the two-layer model agreed best with experimental values. The nanoindentation and two-layer SAW values for E were virtually identical for the thickest film. Discrepancies in other films may be due to acoustoelastic effects or indentation substrate effects.

The two-layer model proved valuable in other cases. In a mini round-robin project for VAMAS TWA 22 begun this year, we examined oxide films (TiO_2 and SiO_2) on glass. SAW measurements on these transparent samples required the addition of a Cr topcoat. The Cr properties were fixed in the two-layer model using results from a sample with a single Cr layer. Preliminary nanoindentation results were in excellent agreement with the SAW results. Also, low-k dielectric films containing secondary capping layers were evaluated with this model (described in detail on the next page of this report).

Although nanoindentation is in widespread use, absolute validation by independent means is needed. The VAMAS project above is one example of our efforts to carefully compare SAW and nanoindentation results. We also performed similar comparisons on a Nb film. In that case, SAW data were obtained at both NIST and another laboratory on the same sample. By combining SAW and nanoindentation information so as to exploit the different sensitivity of each method to different parameters, we obtained a more consistent and complete set of values than possible with either method alone. We will pursue these and related issues (*e.g.*, ultimate uncertainty) during the visit of a guest scientist in late FY03.

Contributors and Collaborators

C. Flannery (Materials Reliability Division, NIST); D. Smith (Ceramics Division, NIST); N. Jennett (NPL, UK); U. Beck (BAM, Germany); D. Fei (Caterpillar)

Physical Properties of Thin Films and Nanostructures: Mechanical Properties of Low-κ Dielectric Films

Although crucial to the microelectronics industry, implementation of low-dielectric-constant (low-κ) films presents serious materials challenges. We apply different optical methods to these films to evaluate their critical properties: density/porosity, Young's modulus, and Poisson's ratio. The techniques provide complementary data and allow measurement of properties that are otherwise difficult to obtain.

Colm Flannery and Donna Hurley

Miniaturization in the microelectronics industry requires lowering the resistance-capacitance (RC) factor in order to achieve faster device switching. This requires replacing standard silica dielectrics with materials of a lower dielectric constant (κ). The most promising way to achieve this is to introduce nanometer-sized pores that reduce κ as porosity increases. An unwanted by-product is a drastic reduction of mechanical properties. The very low Young's modulus of porous low-κ films lessens the chance of their surviving the microelectronic chemical-mechanical polishing process and affects process reliability. Accurate values of film modulus must therefore be known. However, few tools are available to characterize such relevant thin-film properties and their dependence on porosity. Nanoindentation, a standard industry technique, is challenging on such soft films and generally tends to overestimate stiffness significantly. As an alternative, we are developing optical techniques to enable non-contact property measurement.

Brillouin light scattering (BLS) relies on a photon–phonon collision process where incident photons collide with ambient thermal phonons in the material. The frequency shift of the scattered photons, detected by a scanning Fabry–Perot interferometer, is characteristic of the acoustic phonon modes in the film. With BLS, we examined a series of methylsilsesquioxane (MSSQ)
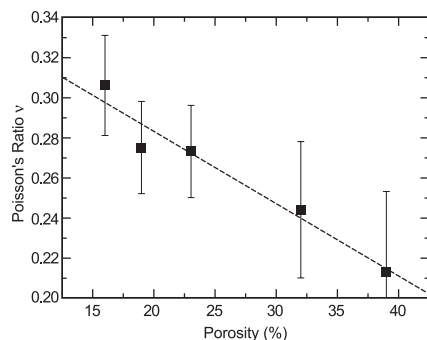
Figure 1: *Poisson's ratio vs. porosity for MSSQ films.*

polymer films of varying porosity. We could detect both longitudinal and surface acoustic wave modes and, thus, could determine values for both Poisson's ratio ν and Young's modulus *E*. Figure 1, which plots the values of ν obtained in these films *vs.* porosity, reveals that ν decreases as porosity increases. This is important since the dependence of n on porosity is not well understood. Very few techniques have been able to provide experimental data to address this issue. BLS appears to be a very promising tool with which to explore this area.
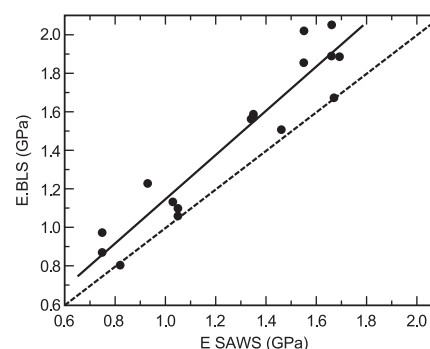
Figure 2: *Young's modulus determined by SAWS and BLS.*

In addition to BLS, frequency-dependent dispersion of laser-generated surface acoustic waves can yield accurate measurements of the density and Young's modulus of thin films. In FY03, we implemented a new SAWS apparatus optimized to inspect thin films on silicon and paid special attention to developing a robust data analysis procedure. Figure 2 compares values of *E* obtained by BLS and SAWS for a range of low-κ films. The results show a clear correlation but with a systematic difference between the techniques of 10–15 %. Reasons for this small discrepancy are being investigated. (SAWS density values have also been verified by x-ray reflectivity measurements).

We are also characterizing two-layer samples (low-κ film with a thin capping layer), interpreted using our newly-developed two-layer Green's function analysis code. Preliminary results show that SAWS is sensitive to the presence of capping layers as thin as 50 nm. Work in the coming year will concentrate on extending SAWS and BLS measurements to multilayer samples, analyzing measurement uncertainties, and developing a standard SAW thin-film data analysis procedure.

Contributors and Collaborators

S. Kim, V. Tewary (Materials Reliability Division, NIST); W. Wu (Polymers Division, NIST); J. Wetzel (Tokyo Electron America)

Physical Properties of Thin Films and Nanostructures: Green's Function Methods

We have developed computationally efficient techniques and computer codes for calculating elastic Green's functions with virtual forces and boundary-element method for application to a variety of elastostatic and elastodynamic problems in advanced materials systems such as semiconductor and metal substrates containing thin layers and nanoinclusions. Many of these codes are available from our library of Green's functions at the NIST website on the Internet.

Vinod Tewary and Bo Yang

Figure 1: *Response to a unit point force normal to the surface of a multilayered piezoelectric solid (InN/AlN). Vertical lines indicate interfaces between adjacent layers.*

Figure 2: *SAW velocity in TiN for $\mu_i = 0.75$ (upper curve), $\mu_i = 1$ (middle curve) and $\mu_i = 1.25$ (lower curve).*

Technical Description

Mathematical modeling of the elastic response of anisotropic materials is required for interpretation and design of experiments leading to industrial applications of advanced materials system such as metals and semiconductors with multilayer coatings or quantum nano-inclusions. The elastodynamic and elastostatic Green's functions (GFs) are used for modeling the propagation of elastic waves, and for calculations of stresses and strains.

We are developing a new defect GF method for elastic response of composite material systems such as thin layers on a substrate or nanoinclusions in a host solid. The defect GF method is well known in discrete lattice statics but is new in continuum mechanics. The traditional technique for solving elastic problems in composite materials consists of solving the equations of elastic equilibrium in different regions and then coupling them with appropriate continuity conditions. We define the defect GF that gives the response of the composite system and seems to be computationally more convenient. The defect GF, denoted by $\mathbf{G^*}$, is related to $\mathbf{G}$; the GF of the host solid through the Dyson integral equation as follows:

$$\mathbf{G^*} = \mathbf{L^{*-1}} = (\mathbf{L} - \mathbf{\Delta L})^{-1} = \mathbf{G} + \mathbf{G}\,\mathbf{\Delta L}\,\mathbf{G^*},$$

where $\mathbf{L^*}$ and $\mathbf{L}$ denote respectively the Christoffel operators of the composite and the host solid, and $\mathbf{\Delta L}$ denotes the change in $\mathbf{L}$ in different regions.

We have extended our earlier GF method for calculating surface acoustic wave (SAW) velocities to multilayered substrates to account for imperfect bonding between the film A and the substrate B by modifying the continuity conditions at the interface as follows:

$$\mathbf{u}_A = \mathbf{\mu}\,\mathbf{u}_B,$$

where $\mathbf{u}$ denotes the displacement at the interface and $\mathbf{\mu}$ is the mismatch tensor (assumed to be diagonal), and the subscripts A and B refer to solids A and B.
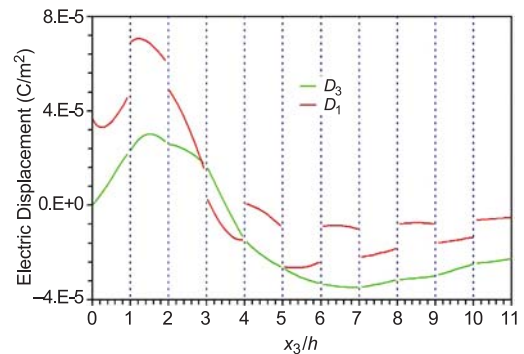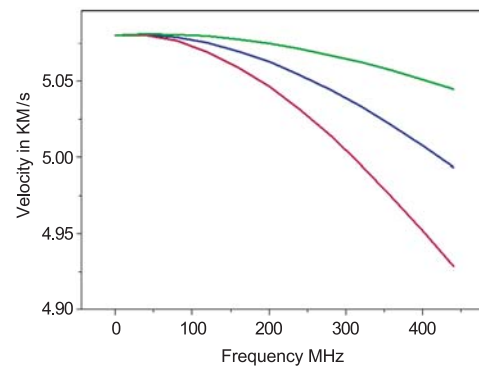
Accomplishments

We have applied our methods to study the formation of surface quantum dots, static response of an anisotropic multilayered piezoelectric structure, steady-state motion of defects in semi-infinite solids and bimaterials, elastic fields due to inclusions in anisotropic half space, and SAW propagation in a TiN film on silicon with a defective interfacial bonding. Computer codes for GF and boundary-element method for a variety of material systems are available for download from our Library of Green's functions at **www.ctcms.nist.gov/gf**. Finally, we have actively collaborated with the formation of the Digital Library of Green's functions in the National Science Digital Library project that was formally launched in December 2002 by the NSF.

Contributors and Collaborators

D. Hurley, R.R. Keller (Materials Reliability Division, NIST); L. Bartlolo (Kent State University); A. Powell (M.I.T.); E. Pan (Akron University)

Micrometer-Scale Reliability: Bridging Length Scales

We have developed a multiscale model for nanostructures in solids. The model relates the physical processes at the interatomic level to measurable lattice distortions at the nanometer level and macroscopic stresses and strains. The model links the subnano (interatomic), nano (nanostructures), and macro length scales by integrating the powerful techniques of molecular dynamics, lattice-statics Green's function, and continuum Green's functions.

David Read and Vinod Tewary

Technical Description

Mathematical modeling is a very important tool for understanding the mechanical behavior of nanomaterials and for research and design of devices based upon nanostructures. A nanostructure needs to be modeled at the following scales: (i) the core region of the nanostructure (sub nanometer) where the nonlinear effects may be significant; (ii) the region of the host solid around the nanostructure (nanometer); and (iii) free surfaces and interfaces in the host solid (macro). A nanostructure causes lattice distortion in the host solid that manifests as strain throughout the solid. The strain is essentially a continuum-model parameter whereas the lattice distortions are discrete variables that must be calculated by using a discrete lattice theory. Hence, one needs a multiscale model that relates the discrete lattice distortions at the microscopic scale to a measurable macroscopic parameter such as strain.

Conventional models of nanostructures are based upon either the continuum theory, which is not valid close to the defect, or molecular dynamics (MD) that is CPU intensive and usually limited to small crystallites, which may introduce spurious size effects. We need a computationally efficient multiscale model that links the length scales from subnano to macro and can be used on an ordinary desktop. Such a model will be a valuable tool for research and engineering designs.

Our model is based upon the lattice-statics Green's function (LSGF) that reduces asymptotically to the continuum Green's function (CGF). However, the response of the solid containing a nanostructure is given by the defect GF that does not reduce to the CGF. The defect GF (**G***) is related to the perfect LSGF (**G**) through the Dyson integral equation:

$$\mathbf{G^*} = \mathbf{G} + \mathbf{G}\Delta\mathbf{\Phi}\mathbf{G^*}.$$

Using the Dyson equation, we can write the response of the defect lattice as a product of an effective Kanzaki force and **G**, which links the perfect LSGF and the CGF.
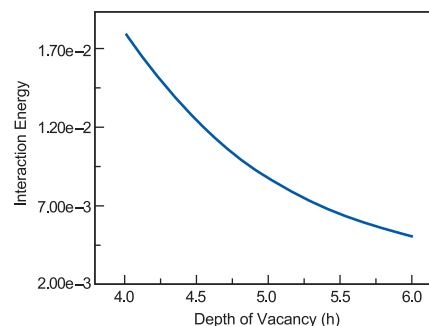
***Figure 1:** Interaction energy (eV) between a vacancy and the free surface in Cu (h in units of a=1.807 Å).*
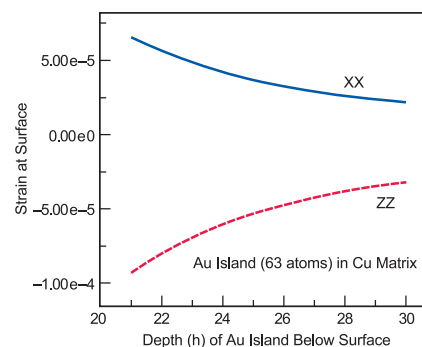
***Figure 2:** Strains at the free surface due to a gold nanoisland in Cu.*

Accomplishments

We have developed a multiscale Green's-function (MSGF) method that integrates LSGF and CGF and applied it to model point defects in metals and semiconductors. This method is suitable for a weak defect such as a vacancy. For modeling nanostructures and other strong defects, we have integrated this method with modified MD in the core of the nanostructure. This integration makes our model truly multiscale by seamlessly linking length scales ranging from the subnano to the macro. Our model accounts for the nonlinear effects in the core of the nanostructure, and it provides a fast algorithm for modeling a large crystallite. It takes only a few CPU seconds to calculate the LSGF for a million-atom model on a standard 3 GHz desktop.

Contributors and Collaborators

R.R. Keller, B. Yang (Materials Reliability Division, NIST); E. Pan (Akron University)

Critical Dimension Metrology of Nanoscale Structures with Small Angle X-ray Scattering

The continued reduction in pattern sizes throughout the semiconductor industry will soon require new metrologies capable of high throughput non-destructive measurements of dense, high-aspect ratio patterns with sub-nanometer resolution. In collaboration with industrial partners, we are developing a metrology based on Small Angle X-ray Scattering (SAXS) to quickly, quantitatively, and non-destructively measure the smallest, or "critical," dimensions expected in the next two technology nodes with sub-nanometer precision. Quantities of interest include critical dimension, pattern sidewall angle, statistical deviations across large areas, and quantitative measures of pattern sidewall roughness. These efforts are driving toward the specification of a laboratory scale device capable of providing pattern dimensions during routine tests of fabrication processes.

Ronald L. Jones and Wen-li Wu

The drive to reduce feature size to the sub-100 nm regime continues to challenge traditional metrology techniques for pattern characterization. Determination of the quality of the patterning process currently depends on the production of test patterns, such as line gratings, and evaluating dimensional control and the number of defects. As pattern sizes decrease, existing metrologies based on scanning electron microscopy and light scatterometry face significant technical hurdles in quantifying pattern dimensions and defects in dense, high-aspect ratio patterns used in modern semiconductor circuitry. There are currently no clear solutions to pattern quality measurement for future technology nodes with dimensions on the order of 30 nm and dimensional control to less than a nanometer.

To address these issues, NIST is developing a transmission x-ray scattering-based method capable of angstrom level precision in critical dimension evaluation over large, (50 x 50) μm, arrays of nanoscale periodic structures. In contrast to light scatterometry, Small Angle X-ray Scattering (SAXS) is performed in transmission using a sub-Angstrom wavelength. With a wavelength more than an order of magnitude smaller than the pattern size, the patterns can be analyzed using methods traditionally employed in crystallographic diffraction. The high energy of the x-ray beam allows the beam to pass through production quality silicon wafers without requiring a specialized

sample environment (ultrahigh vacuum). While current measurements utilize the flexibility and wide array of instrumentation available at a synchotron source, initial results and the commercial availability of x-ray sources and detectors suggests the technique is portable to a laboratory scale device.

As shown in the schematic below, the patterned sample is placed in an x-ray beam where the transmitted intensity is measured as a function of the scattering angle, 2θ, on a 2-D detector. The intensity is then fit to models describing the average pattern shape. To save valuable space within the total patterned area, industrial test patterns are typically smaller than (50 x 50) μm. Using a monochromator to define the wavelength and two sets of beam-defining slits, beam footprints of approximately (40 x 40) μm have been successfully demonstrated. In contrast to 1-D techniques such as light scatterometry, the use of a 2-D detector allows the simultaneous characterization of all dimensions for patterns such as vias (arrays of cylinders standing perpendicular to the surface) and via pads (arrays of rectangles). In addition to measuring the pattern dimensions along the substrate plane, measurements at varying sample rotation angles, ω, can be used to reconstruct the average 3-dimensional pattern shape.
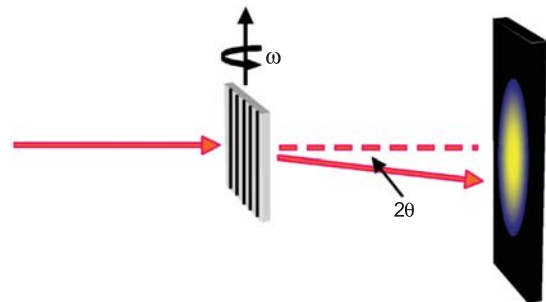
Figure 1: *Schematic of SAXS geometry, showing incident and scattered beams (red lines), sample with pattern oriented at rotation angle ω and 2-D detector (right).*

In collaboration with International SEMATECH, recent SAXS measurements of line gratings have demonstrated the capability of SAXS to measure fabricated patterns of thermally grown oxide with overall dimensions designed for current metrologies. The resulting detector image is a series of diffraction peaks along a single diffraction axis perpendicular to the orientation of the grating. The number of observable diffraction orders is in part determined by the pattern quality. The observation of over 30 orders of diffraction suggests the relatively high quality of these patterns and provides ample data for

high-precision analysis. In addition, the number of observable diffraction orders serves as an immediate measure of pattern quality, termed a SAXS "fingerprint." With a measurement time on the order of a second, dose exposure matrices commonly used to evaluate optical imaging conditions can potentially be evaluated in a matter of minutes.

In addition to the SAXS "fingerprint," quantitative information is obtained through model fitting of the data. In contrast to reflection-based techniques, the models used here are relatively simple. Quantitative measures of the pattern repeat period and the line width are therefore obtained rapidly and precisely. For these samples, SAXS data have provided sub-nanometer precision in both average repeat distance and average line width. The precision of this measurement is in part dictated by the number of observable diffraction orders, which is in turn limited by the instrumental resolution and pattern quality. Ongoing studies will compare these results with measurements from light scatterometry, atomic force microscopy, and scanning electron microscopy.

In collaboration with the IBM T.J. Watson Research Center, the effects of specific types of defects in patterns on the resulting SAXS image are being explored. Shown in Figure 2, a simple model of an ideal line grating captures the main features of the diffraction spots; however, additional information
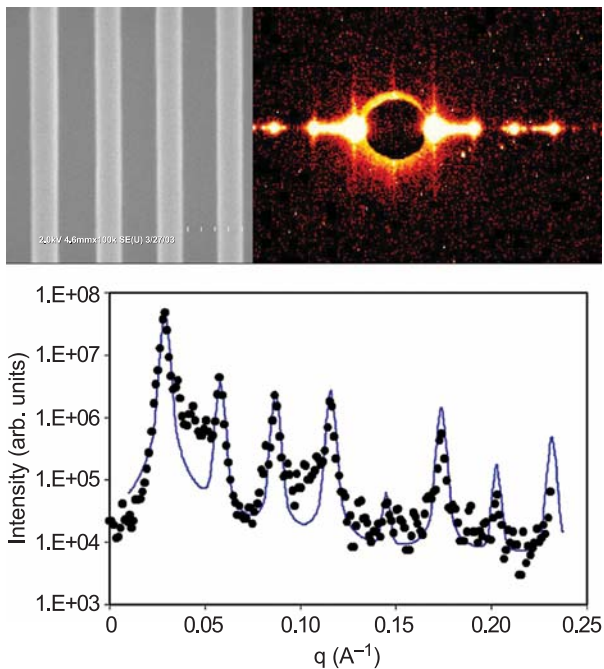
is observed in the 2-D image perpendicular to the diffraction axis. Streaks of intensity emanating from diffraction peaks are visible near the beamstop. These streaks are indicative of deviations from the ideal grating and may provide information about defects such as long wavelength line edge roughness.
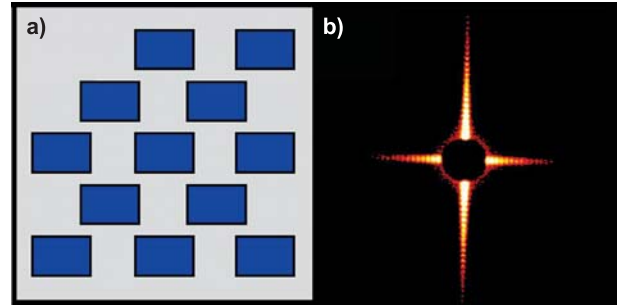
Figure 3: *Schematic of via-pad patterns (a), where the blue rectangles represent etched regions in a low-k film, and (b) the resulting SAXS detector image.*

In addition to precisely measuring dense patterns of etched silicon oxide, the application of SAXS has been demonstrated for a wide range of materials that are currently used or are being explored for use in the microelectronics industry. We demonstrated the capabilities of SAXS on dense patterns of organic photoresist, silicon oxide, and nanoporous low-k samples (detector image from 2-D array of via pads shown in Figure 3). Additionally, measurements on samples of copper-filled, low-k patterns demonstrate the capability to probe multiple component and metallic patterns. Finally, the transmission geometry allows the probing of densely packed structures, whether buried or exposed, providing a potential to measure other nanoscale 3-D structures being explored for future microelectronic devices and photonic crystals.

Continuing efforts will focus on developing quantitative measures of line edge and sidewall roughness, isolating specific types of long-range order defects arising from masks, and reconstructing an average 3-D pattern shape. In addition, further investigations will provide precise specifications for a laboratory scale device capable of similar measurements.

Figure 2: *Top down SEM image (top left) of a photoresist grating on a silicon wafer compared to the resulting 2-D SAXS image (top right). Also shown are the intensities of the diffraction peaks as a function of scattering vector, q ($=4\pi/\lambda \sin\theta$, where λ is the x-ray wavelength) fit with a simple model (solid blue line).*

For More Information on this Topic

R. Jones, T. Hu, W. Wu, E. Lin (Polymers Division, NIST); G. Orji, T. Vorburger (Precision Engineering Division, NIST); A. Mahorowala (T.J. Watson Research Center, IBM); G. Barclay (Shipley Co.); D. Casa (Advanced Photon Source, Argonne National Laboratory)

R.L. Jones, T.J. Hu, E.K. Lin, W.-L. Wu, D.M. Casa, N.G. Orji, T.V. Vorburger, P.J. Bolton, G.G. Barclay, *Proc. SPIE* **5038**, 191 (2003).

Elastic Flow Instability in Polymer-Dispersed Carbon Nanotubes

Novel composites engineered from polymers and carbon nanotubes offer the promise of plastics with enhanced thermal, electronic, and mechanical properties, but the ability to control and quantify particle dispersion in such materials is an unresolved issue of fundamental importance. Of particular interest is how processing flows influence tube dispersion and orientation. We are developing metrologies and methods that directly address the fundamental nature of elastic flow instabilities in polymer-dispersed carbon nanotubes, enabling better control of dispersion during flow processing of melts and suspensions.

Erik K. Hobbie

The clustering of small spherical particles has been studied extensively in a broad range of systems. In contrast, relatively little is known about the flocculation of asymmetrical particles, such as platelets, rods, or fibers. Given the current interest in dispersing anisotropic nanoparticles in organic materials to enhance physical properties, a deeper understanding seems warranted. An almost universal aspect of aggregation is inter-particle attraction, but external hydrodynamic forces, often used to disperse such particles, can alone induce clustering in highly *anisotropic* suspensions, creating unique challenges and issues relating to the flow processing of such materials.

We recently observed an elastic instability associated with flow-induced clustering in polymer dispersed carbon nanotubes. Kinetic measurements under varied confinements and shear stresses were compared with simulations of flocculation in flowing fiber suspensions, and we found an intriguing rheological signature consistent with highly elastic domains. Small-amplitude oscillatory shear measurements reveal this extraordinary elasticity, with homogenized semi-dilute suspensions showing gel-like behavior at long time scales. The data suggest that the underlying instability may in fact be universal to a number of flowing complex fluids, with important implications for the flow processing of polymer-carbon nanotube composites.

Multi-walled carbon nanotubes (MWNTs) were grown via chemical vapor deposition. A typical electron micrograph is shown in the inset to Figure 1(a). Based on such measurements, the mean diameter is $d \approx 50$ nm. Due to their length and optical contrast, individual MWNTs are discernable in optical micrographs of 25x or higher, and from 200x images of thin-film dispersions,

the mean length is $L \approx 12$ µm. The suspending polyisobutylene fluid (PIB) is Newtonian over a broad range of shear rates, with a shear viscosity of 10 Pa-s at 25 ºC. Dispersions are prepared by dissolving the PIB in sonicated MWNT-toluene suspensions, which are stirred continuously as the solvent is removed. Suspensions of primary interest contain 1.7×10^{-3} mass-fraction MWNT in PIB and are semi-dilute, with $nL^3 \approx 45$ and $nL^2d \approx 0.19$, where n is the number of tubes per unit volume. The tubes in PIB are non-sedimenting over the time scales in question.
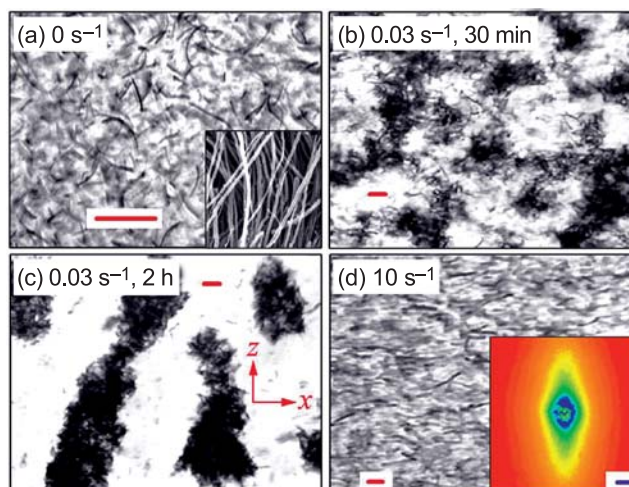
Figure 1: *(a) Optical micrograph of MWNTs in a quiescent PIB dispersion. The inset (width = 1.3 µm) is a SEM image of the MWNTs before dispersion in PIB. (b) Optical micrograph 30 min after quenching the mixture to a shear rate of $\dot{\gamma}_o = 0.03\ s^{-1}$. The flow (x) direction is horizontal. (c) Optical micrograph 2 h after the quench. (d) Optical micrograph 15 min after quenching the sample in (c) to $\dot{\gamma}_m = 10\ s^{-1}$.*

Optical microscopy (5x to 25x) is used to observe the motion of MWNTs and the formation of aggregates under shear, with flow along the x-axis, a constant velocity gradient along the y-axis, and vorticity along the z-axis. Measurements are taken in the x–z plane. The sample is confined between two parallel quartz plates separated by a variable gap, h. The upper plate rotates at an angular speed that sets the shear rate, $\dot{\gamma} = \partial v_x/\partial y$, at a fixed point of observation in the middle of the plates. A controlled-strain rheometer in cone-and-plate and parallel-plate configurations provides steady and oscillatory shear measurements of the rheology. All measurements were performed at 25 ºC.

The aggregates have "melted" and the redispersed tubes broadly orient with the direction of flow, as evident in the light-scattering pattern (inset Figure 1(d), scale bar = 1 µm^{-1}). The scale bar is 10 µm and the gap (h) is 70 µm.

Under weak shear, the tubes form macroscopic domains consisting of diffuse MWNT networks. Figure 1 shows optical micrographs of (a) a quiescent dispersion, (b & c) aggregation at $\dot{\gamma}_o = 0.03$ s^{-1}, and (d) redispersed MWNTs after dissolution at $\dot{\gamma}_m = 10$ s^{-1}, where light scattering reveals a steady-state distribution of orientations broadly peaked around $\hat{\mathbf{x}}$. In simple shear, the long axis of an isolated rod rotates around $\hat{\mathbf{z}}$ with a period, τ, that scales as $\dot{\gamma}^{-1}$. In semi-dilute suspensions, hydrodynamic interactions determine the distribution of such orbits. The Peclet number is less than 10^{-4}, implying that hydrodynamic forces overwhelm Brownian forces.
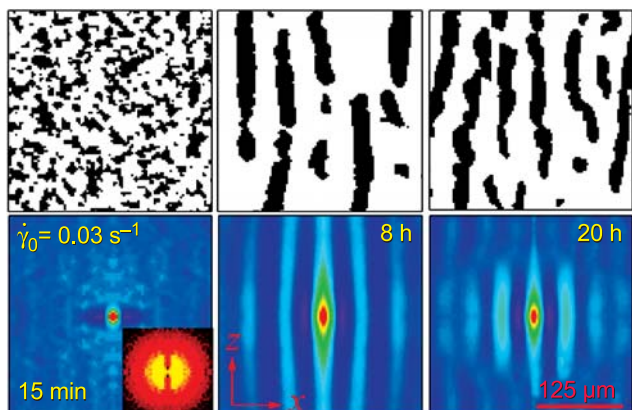
Figure 2: *Evolution of a confined dispersion (upper), where the micrographs have been converted to binary images. The lower images are the corresponding c(r). The flow direction is horizontal, the vorticity axis is vertical, and the red scale bar (125 μm) applies to all six images. As in Figure 2, h = 70 μm. The inset to the lower left image is its FFT (width = 1.2 μm^{-1}), which gives the ubiquitous "butterfly" pattern.*

By varying h, we observe the transition from bulk to confined growth. To quantify the latter, we convert micrographs into binary images in which the clusters are black and the surrounding fluid white (upper images, Figure 2), defining a coarse composition field $\psi(\mathbf{r})$. Ensembles at each annealing time, t, are used to compute the two-point correlation function, $c(\mathbf{r}) = \langle \psi(\mathbf{r})\psi(0) \rangle$ (lower images, Figure 2), and the steady-state morphology diagram in the $h - \dot{\gamma}$ plane is shown in Figure 3. In region A, moderate aspect ratio domains exhibit broad vorticity alignment. In region S, these domains coarsen along $\hat{\mathbf{z}}$ into macroscopic striped patterns. The dashed curve marks a region of "metastability" in which the striped pattern is transient.

Recent simulations of flow-induced flocculation in non-Brownian fiber suspensions suggest that inter-particle friction leads to aggregation in the absence of attractive interactions, particularly at low-shear stress and high-fiber stiffness. The MWNT bending modulus can be compared with values for typical organic fibers, as can the shape of the inter-particle potential and

coefficient of friction. Our measurements are in agreement with simulation. With an elastic bending modulus 10^3 times larger than that of a typical fiber, the MWNTs are flexible enough to exhibit shape deformation, yet they readily entangle and interlock to form large coherent structures under weak shear. Held together by elastic forces, the diffuse clusters store sizeable energy, which we infer from linear viscoelastic measurements of the storage modulus, $G'(\omega)$, as a function of n. Other unusual features, such as a negative first normal stress difference, are currently under in-depth investigation.
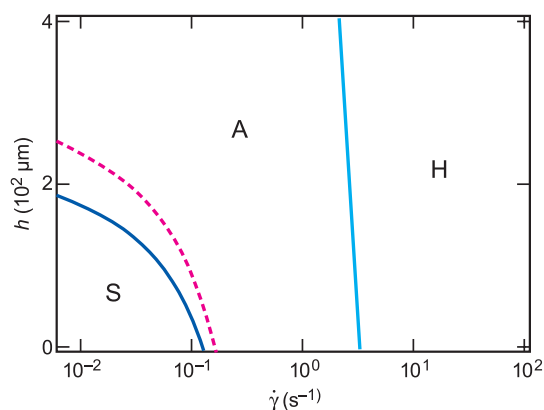
Figure 3: *The measured late-t "pattern diagram" in the $h - \dot{\gamma}$ plane for the semi-dilute, non-Brownian MWNT-PIB suspensions of interest, with homogeneous (H), aggregated (A), and "striped" (S) regions as indicated.*

We have observed the early-time domain pattern [Figure 2 (left), weak minima in $c(x)$] in a host of flowing complex fluids, including polymer blends, semi-dilute polymer solutions, physical polymer–clay gels, and thixotropic clay gels, all of which fall within the simple paradigm of weakly interacting elastic domains suspended in a less viscous fluid. The homogenized semi-dilute dispersions also exhibit solid-like behavior at long timescales, suggesting the presence of a weak "network" or gel, further reminiscent of other systems that exhibit this type of flow-induced macrostructure. The role of confinement in the growth of periodic structures in these systems is intriguing and merits detailed computational consideration. We expect that these issues will have direct consequences for the processing of nanocomposite melts, and we are currently extending these measurements to single-walled carbon nanotubes.

For More Information on this Topic

E.K. Hobbie, S. Lin–Gibson, J. Pathak (Polymers Division, NIST); H. Wang (Michigan Tech); E. Grulke (University of Kentucky)

Multiscale Modeling of a Gold Nanoisland in a Million-Atom Copper Crystallite

Modeling and simulation are playing key roles in the discovery and interpretation of nanoscale and atomic-scale phenomena. Multiscale modeling is the most efficient way to include surfaces accessible for measurements in models of atomic-scale phenomena. The brute-force approach would require treating millions or even billions of atoms explicitly. A copper cluster of 1 billion atoms has a side of only 0.23 micrometers, so the desirability of the multiscale approach is clear.

Vinod Tewary and David Read

Our multiscale modeling approach combines molecular dynamics (MD) with a recent extension of Green's function (GF) analysis. We divide the physical system to be analyzed into a core, where the strong, non-linear interactions of interest occur, and an outer core, a shell and a host solid, where the atomic interactions become progressively more linear (termed "harmonic") and the strains decrease to elastic levels. Harmonic behavior can be treated with much less effort, and much less computer power, than nonlinear atomic interactions. In the core, MD is used to maintain the capability to treat strongly nonlinear interactions. The outer core is the region where all the atoms are near their perfect-lattice positions. The core atoms are contained by the shell atoms, which are shared between the MD and GF models, but controlled by the harmonic interactions described by the GF. Outside the shell, the atoms blend into the continuum. Surfaces, with associated strains and displacements, can be placed in the harmonic-lattice or continuum GF regions.

We selected the vacancy in copper as our initial problem to develop and test the method; then we applied the method to a gold nanoisland in a copper matrix. The energy of the vacancy turns out to depend only very weakly on the size of the crystallite considered, so problems in the multiscale approach would have shown up clearly. Even as late as the 1960s, the energy of formation of a vacancy had not yet been calculated accurately. Damask and Dienes, writing in 1963, list values from 0.81 to 1.2 eV. The latest experimental value is given by Wollenberger to be 1.28 ± 0.05 eV. The energy of formation of the vacancy could not be evaluated properly using the pairwise atomic interactions developed during the 1970s and 1980s. However, in the late 1980s and early 1990s, workable many-body potentials were developed.

These potentials, fitted to experimental elastic constants, produced accurate vacancy energy values. Here we use a "second moment–tight binding" potential reported by Cleri and Rosato in 1993. It is a very long-range potential, out to fifth neighbors, and parameters were given for mixtures of gold and copper, as well as for the elements individually.

The MD method can evaluate the formation energy of the vacancy; of course, the result depends on the parameters of the MD model used, and the vacancy energy is often considered in fixing the parameters. Both the MD and GF models can calculate the displacements that occur when an atom is removed from a crystallite to create a vacancy. We carried out such calculations with the MD and GF models separately, and they agreed. Then we combined them in the multiscale approach. The multiscale calculation for 216,000 atoms converged after only one iteration. Figure 1 shows the relaxation, and also shows that the strains caused by the vacancy are concentrated in the 100 or so atoms nearest the vacancy. The energy of formation of the vacancy includes these deviations from the perfect-crystal energy.
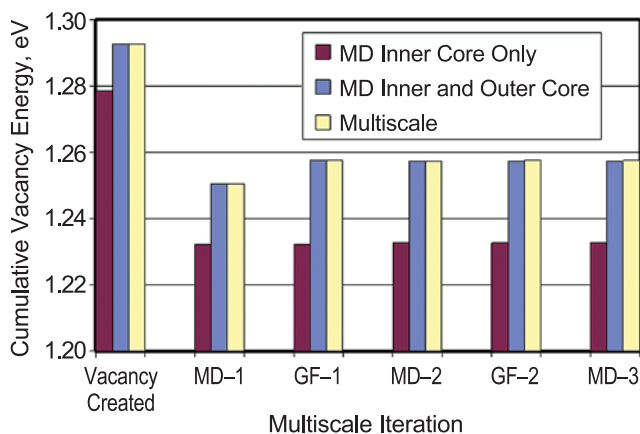
Figure 1: *Multiscale model evaluation of the energy of a vacancy in a copper lattice. The vacancy is created, then the configuration relaxes iteratively to its minimum energy configuration. The MD core contribution to the energy is the largest, because it includes the missing interatomic bonds. Strains in the outer core and the host add to the energy. The latest published experimental result is 1.28 ± 0.05 eV.*

The MD and GF models cooperate closely in the multiscale calculation. The MD model controls the core atoms, and calculates forces on the shared atoms, which are regarded as fixed within the MD calculation. The GF model, in turn, calculates displacements for the shared and outer-core atoms. Because the potential is

many-body, the force on an atom depends on the position of all its neighbors. This dependence is especially pronounced in the fifth neighbor Cleri–Rosato potential used here. The key mathematical "trick" of our multiscale approach is that the many-body force contributions from the host atoms, which are not included in the MD model but are required to get the forces on the shell atoms correct, are evaluated using the equilibrium conditions enforced by the GF model for the outer core, shell, and host regions. As the minimum energy condition is approached, the atomic displacements are smaller so that eventually these forces become constant and the iteration converges.

By replacing 63 atoms within a million-atom copper lattice with gold atoms, we created a gold nanoisland within the copper matrix. Gold's face-centered-cubic (fcc) unit cell is 13 % larger than that of copper; the unknowns were how much the expansion of the gold island would be restrained by the surrounding copper, and what form of the strain and displacement fields around the gold island would be. These turned out to be surprisingly complex. Because the GF model includes the capability to account for a free surface, these strains and displacements are experimentally accessible using, for example, scanned probe microscopy (SPM) or local x-ray diffraction (XRD). This simulation required a larger MD core and shell than the vacancy. We placed 10,156 atoms in the shell and 5,356 in the outer core. Figure 2 shows the initial and final positions of atoms on a section through the gold nanoisland.
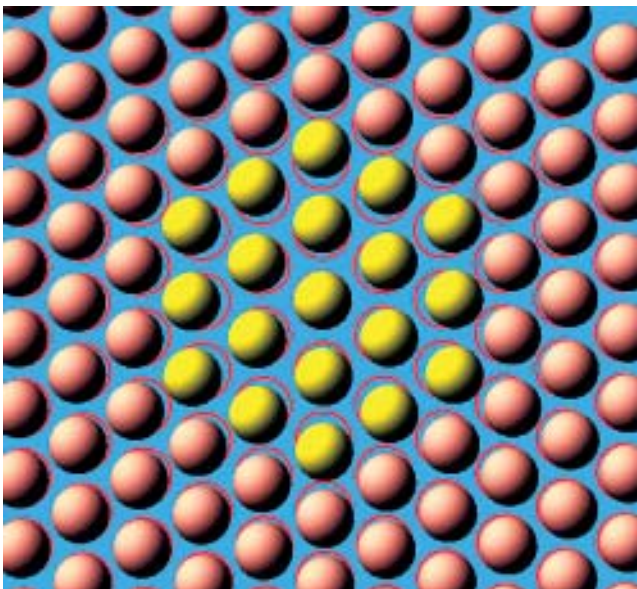
Figure 2: *Section through gold nanoisland in copper after partial relaxation. The red circles indicate the original positions of the copper lattice sites. Note the short range of the displacement field around the nanoisland. The copper nearest-neighbor distance is 2.55 Å.*
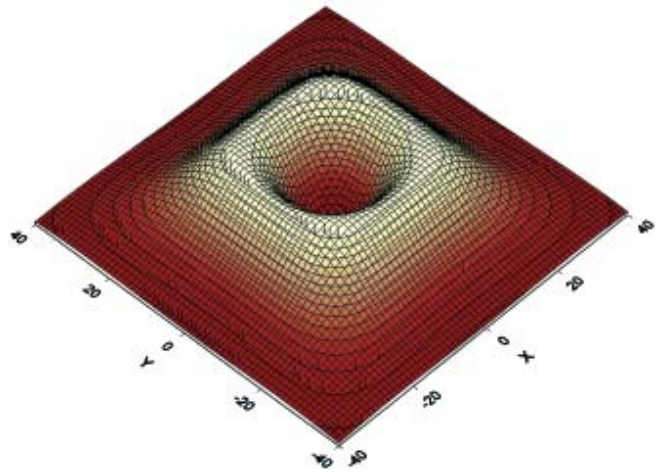
Figure 3: *Out-of-plane surface displacements above an 8 Å-wide gold nanoisland located 38 Å beneath the surface of a million-atom copper lattice. The maximum height is 0.02 Å.*

The gold nanoisland was placed near a surface to calculate surface strains and displacements. Figure 3 shows the out-of-plane displacements. The largest displacement does not occur directly above the nanoisland. Rather, the displacement peaks at the same distance out from the center as the nanoisland is beneath the surface. That the displacement is upwards above the nanoisland is consistent with the larger lattice parameter of gold, compared to copper.
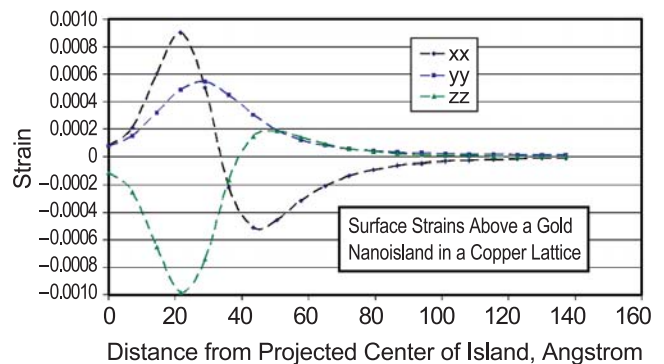
Figure 4: *Surface strains above an 8 Å-wide gold nanoisland located 38 Å beneath the surface of a million-atom copper lattice.*

Figure 4 shows the surface strains above the island. The surface strains above the nanoisland are even more complex than the displacements because of the elastic anisotropy of the copper elastic constants.

For More Information on This Topic

V. Tewary, D.T. Read (Materials Reliability Division, NIST)

Gradient Combinatorial Reference Specimens for Advanced Scanned Probe Microscopy

Engineering of nanomaterials, biomaterials and NEMS hinges on characterization techniques that image complex nano-scale structures. In this respect, new Scanned Probe Microscopy (SPM) methods promise to provide nano-scale mapping of chemical, mechanical, and electro-optical properties. However, emerging SPM techniques generally offer qualitative information since probe fabrication is inconsistent and since probe/sample interactions are not understood. Through a suite of reference specimens fabricated with a combinatorial design, we aim to gauge probe quality and calibrate advanced SPM image contrast, thereby advancing these promising tools for nanometrology.

M.J. Fasolka, D. Julthongpiput, and P.M. McGuiggan

Introduction

Scanned Probe Microscopy (SPM) techniques promise micrographs that map specimen properties with nanometer scale resolution. While current SPM images generally afford qualitative information, some progress has been made in quantifying SPM data. A prime example in this regard is AFM topography data. In this case, two factors, scanning piezo non-linearity and unknown probe tip shape, hamper precision measurements of specimen surface features. Now, linearized/calibrated piezo systems ensure micrograph dimensions. In addition, specialized substrates with ultra sharp features can measure tip geometry so that, in principle, tip-shape effects on topographic data can be removed. Indeed, such reference specimens are now available commercially.

In recent years, a new generation of SPM techniques, which intend to measure chemical, mechanical, and electro/optical properties on the nanoscale, have been developed. Based upon sample/probe interactions that are more complex than in AFM, contrast in these new SPM images is difficult to quantify. In particular, the development of quantitative SPM techniques requires methods to gauge the following factors:

- *Resolution and Sensitivity*: The lateral resolution, measurement volume, and sensitivity to measured properties must be determined.

- *Probe Quality*: Many new SPM techniques depend upon custom-made probes, the fabrication of which often is not reliable or uniform. Accordingly, convenient means to characterize these probes are needed.

- *Combination Effects*: SPM measurements of, for example, chemical properties are convoluted with local mechanical, topographic, and other effects. Effective reference specimens would serve to separate the impact of these "combined" effects on image contrast.

In response to these needs, a new research effort initiated by the NIST Combinatorial Methods Center (NCMC) aims to provide a suite of reference specimens useful for the quantification of next-generation SPM data. By design, these specimens gauge the quality of SPM probes, calibrate SPM image contrast through "traditional" surface measurements (*e.g.*, spectroscopy, contact angle), and provide information useful for modeling complex probe/sample interactions. The design and production of these specimens uses bench-top microfabrication routes, used in conjunction with the combinatorial gradient-specimen fabrication toolbox developed by the NCMC. Here, the use of combinatorial methods is key, since these approaches can fabricate specimens that vary properties expected to govern SPM image contrast in a gradual and independent manner.

Reference Specimen Design
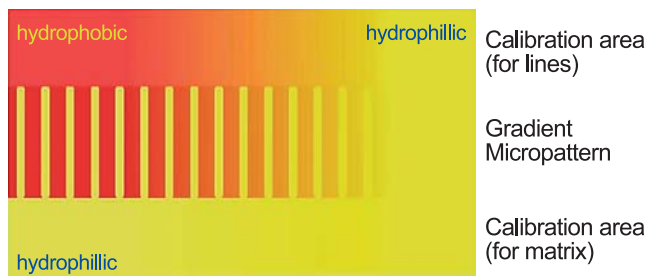
Figure 1: Schematic of gradient reference specimen for gauging tip quality, for calibrating image contrast, and for determining sensitivity in chemically-sensitive SPM techniques. Chemical contrast in the patterned area is gauged via traditional measures along the calibration areas.

An example reference specimen design is illustrated in Figure 1. Such a specimen would be useful for quantifying chemically sensitive SPM techniques such as friction-force AFM or Chemical Force Microscopy (CFM), which employs a chemically

functionalized AFM probe. The reference specimen includes a pattern of micron-scale lines that gradually change in their chemical contrast (*e.g.*, surface energy) with respect to a constant matrix. Wide "calibration" fields, which bound the patterned area, directly reflect the changing (or static) chemistry of the lines (or matrix); so traditional measurements along the calibration fields gauge chemical differences in the gradient micro-pattern. Accordingly, for SPM micrographs acquired along the patterned region, the specimen calibrates the image contrast and illuminates the sensitivity (minimum contrast) with respect to traditional measures. In addition, for techniques like CFM this specimen serves as a tool for comparing the quality of tip-functionalization.

Example Route
For Specimen Fabrication

Fabrication of gradient-pattern specimens requires soft-lithography of appropriate SAM molecules onto a planar substrate. A composite stamp, which has both flat and corrugated areas, allows printing of the micropatterned strip with the adjacent solid calibration field. Next, a graded UV-ozonolysis (UVO), gradually modifies the chemistry of the patterned SAM (and calibration field) along one direction. For example, methyl-terminated alkyl chain monolayers (hydrophobic) can be gradually converted into carboxylic acid terminated (hydrophilic) chains. Subsequent "filling" with a hydrophilic SAM completes the "matrix" of the specimen. To test this design and process, traditional micro-contact printing of thiol-SAM "inks" onto gold substrates followed by

gradient UVO provided quality specimen prototypes. While this validated the specimen design, ultimately the use of delicate gold / thiol chemistry will not result in specimens that can be stored, cleaned, and reused. Accordingly, the next generation of reference specimens will be fabricated using more robust substrates and chemistries, thereby making them viable candidates for applications such as NIST Standard Reference Materials.

In the beginning stages of this project, we will demonstrate novel routes for the graded patterning of monochlorosilane (MCS) SAMs on SiO_2-terminated silicon substrates; and we will discuss the fabrication and testing of reference specimens created through these new fabrication approaches. The utility of these specimens will be demonstrated with respect to emerging SPM techniques such as CFM and Atomic Force Acoustic Microscopy. In addition, we will show how graded pattern specimens can be useful for the high-throughput analysis of surface-directed behavior in thin films of homopolymers, polymer blends and block copolymers.

For more information on NCMC SPM research and combinatorial methods in MSEL, see **www.nist.gov/combi**.

Contributors and Collaborators

D. Hurley (Materials Reliability Division, NIST); B. Huey (Ceramics Division, NIST); T. Nguyen, X. Gu (Materials and Construction Research Division, NIST)

Bridging Length Scales in Theory and Modeling: Microstructure Evolution and Material Mechanics

The performance of many structural and functional materials depends on the distribution of composition, phases, grain orientations, internal stresses, and microstructure on length scales from nanometers to meters. Industry needs predictive models to reduce the enormous costs and development times involved in designing and inserting new materials into state-of-the art products. To address these needs, we are developing phase field models of solidification and solid-state transformations, with coupling to stress, grain orientation and solute/vacancy dynamics.

James A. Warren and William J. Boettinger

In order to model the complex interfacial shapes that produce real microstructures, the phase field method has become the technique of choice for computational materials scientists.

Modeling of microstructures produced by processing of materials involves solution of mathematical equations for heat flow, deformation/fluid flow, and/or solute diffusion. Boundary conditions on external surfaces reflect the macroscopic processing conditions that can be externally controlled. In classical models of materials processing, boundary conditions on internal interfaces corresponding to the liquid–crystal (grain), grain–grain and/or phase–phase interfaces reflect material thermodynamic and kinetic conditions. For solid–solid transformations, stress effects also become significant, and surface stresses become particularly important in nanoscale microstructures. Phase field models finesse the difficult numerical task of tracking moving internal interfaces by the introduction of a new variable, the phase field.

Research in phase field modeling conducted in the Metallurgy Division is also supported by the NIST Center for Theoretical and Computational Materials Science. Recent efforts have focused on bringing together many of the disparate efforts in phase field modeling to create a unified picture of materials processing with a single set of equations governing microstructure evolution. In the past year we have:

- Developed a model of a stressed system containing a curved interface between two phases with different elastic properties. This model has been applied to a liquid (zero shear modulus)–solid system.

- Simulated 3-D fault dynamics in directionally solidified binary eutectics.

- Combined phase field models of eutectic colony growth with polycrystalline structures. This approach readily deals with complex interface shapes and topology changes (see Figure 1).

- Simulated the growth of dendrites in polymers where crystallographic rotation of the growth direction occurs, "dizzy dendrites" (with the Polymers Division).

- Prepared an overview of phase field modeling of polycrystalline growth and coarsening (*Acta Materialia*, in press).
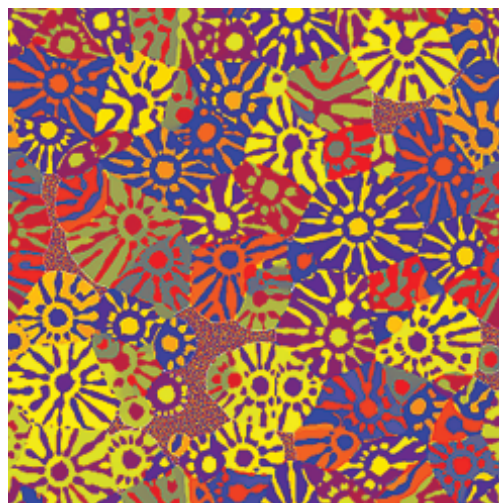
Figure 1: *A simulation of eutectic colony growth. The colors indicate crystal orientation. The solid phase can be distinguished as large regions of a single color while the liquid appears essentially random in orientation at the smallest scales.*

While this research is ambitious in its scale, the successes so far suggest that the goals are within reach. Work to be done includes joining the stress models with existing models of polycrystalline growth, the addition of vacancies to all of these models in a thermodynamically consistent manner, the extension of the grain boundary model to three dimensions, and the coupling of all of these effects to fluid flow.

Contributors and Collaborators

J. Warren, W. Boettinger, D. Lewis, J. Guyer, R.F Sekerka (Metallurgy Division, NIST); J. Douglas (Polymers Division, NIST); J. McFadden (Mathematical and Computational Sciences Division, NIST); J. Slutkser, A. Roytburd (University of Maryland); R. Kobayashi (Hokkaido University, Japan); L. Granasy (RISSPO, Hungary)

Particle Metrology and Standards

As technology migrates toward smaller physical dimensions, new analytical approaches are required to characterize material properties and to investigate scientifically important issues. In particle technology, these needs become critical in the nanosize regime. Industrial processes involving nanoparticle technology include advanced device manufacture and the development and production of functional materials for microelectronic, pharmaceutical, and biotechnology applications. Our goal is to improve existing metrology and develop new methods and standards for measuring the physical and interfacial properties of nanosize and nanostructured particle systems.

Vincent A. Hackley and James Kelly

Standard reference materials (SRMs) are critical for calibrating instruments used for nanoparticle characterization. Primary customers for nanoparticle SRMs are quality control laboratories in the ceramic and pharmaceutical industries. This year, we have initiated the production of a 100 nm to 500 nm particle size distribution (PSD) SRM, the first of its kind (inorganic material system with a broad size distribution), to fulfill a pressing need in the sub-micrometer size range. Interest in this TiO_2-based standard has been expressed from a wide range of industries. The SRM will be certified for PSD using electron microscopy and by X-ray disc centrifuge methods. Additionally, certification of SRM 1021 was completed. This SRM is intended for the evaluation and calibration of equipment used to measure PSDs in the 2 µm to 12 µm diameter range. The size range of this SRM follows that of the coarser beads of existing SRM 1003c.

Another activity involves ultra-small angle x-ray scattering (USAXS) of nanoparticle suspensions and partially-gelled systems. Objectives are to develop sensitive metrological techniques for characterizing metastable and unstable nanoparticle suspensions and to gain new insights into mechanisms influencing their agglomeration and stabilization. Systems of interest include SiO_2, TiO_2, and ZrO_2, studied after stabilization at pH values representing states close to and far from the isoelectric point. For example, Figure 1 shows discrete particle doublets (right-hand peak) in SiO_2 suspensions that form only at the isoelectric pH. USAXS allows such phenomena to be quantified to an unprecedented level. A flow cell for *in situ*, real-time USAXS studies of unstable suspensions is under development.
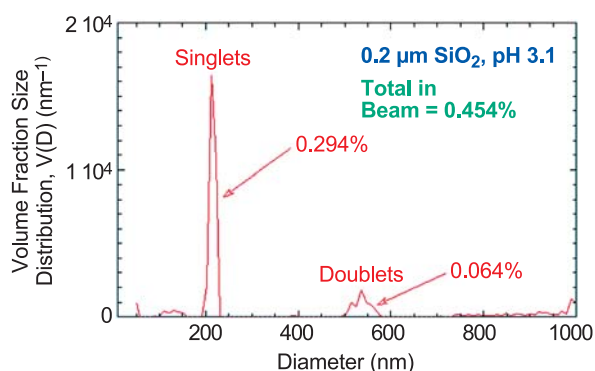
This year, a new activity was initiated on interfacial property measurements of nanostructured particulates. The goal is to develop the measurement methodology to obtain reliable data to establish a clear relationship between charge development and particle size, crystallinity and interparticle structure. Metal oxides exposed to an aqueous phase develop charge via protonation of surface hydroxyl sites. Surface charge and surface site reactivity play key roles in dissolution, precipitation and growth, corrosion, aggregation, and sorption processes. As particle size shrinks into the low nano-regime (< 10 nm), charge development and reactivity are predicted to exhibit size dependent behavior. Preliminary results indicate some potentially important findings.

- A systematic decrease in the isoelectric point of TiO_2 with decreasing crystallite size was observed; data will be incorporated into modeling efforts by NSF-funded researchers to account for proton-induced charge formation as a function of crystal size.

- Zeta potential measurements indicate that adducts formed between nanocrystalline MgO and molecular halogen species are more stable in an aqueous medium than had been previously predicted; this has important implications for their use as microbial biocides.

- Small-angle neutron scattering experiments suggest MgO may be capable of localized expansion around individual crystallites in response to an aqueous intrusion, without fully disrupting the assembly structure; this would represent a unique attribute not typically associated with inorganic particles.

Figure 1: *Volume fraction PSD for SiO_2 at the isoelectric point.*

Contributors and Collaborators

A. Allen, A. Jillavenkatesa, L. Lum (Ceramics Division, NIST); L. Sung, C. Ferraris (Materials & Construction Research Division, NIST); D. Ho (Center for Neutron Research, NIST); K. Klabunde (Kansas State University); U. Paik (Hanyang University); M. Ridley (Texas Tech University); M. Machesky (Illinois State Water Survey); P. Jemian (University of Illinois)

Metrology for Nanoscale Properties: Conductive AFM Using Carbon Nanotubes

The latest integrated electrical circuits, as well as microelectical mechanical devices, are dependent on sub-micron features with very high aspect ratios. We are developing a technique using carbon nanotubes mounted to atomic force microscope tips to probe the surface conductivity of these devices with nanometer resolution. The development of these tips also leads to probing high-frequency electronic circuitry and the electrical properties of biological specimens.

Paul Rice

We are mounting carbon nanotubes on the end of conductive atomic force microscope (AFM) tips to probe the surface electrical properties of various samples with nanometer resolution. Using these tips, we are attempting to map the sample surface conductivity and also to probe local electric fields on high-frequency circuits.

Carbon nanotubes have qualities that make them very desirable as AFM probes. They can be micrometers long and only nanometers in diameter allowing for probing devices with deep narrow

features such as microelectrical and mechanical systems (MEMS). In addition, there are a variety of types of nanotubes that can have different electrical transport properties. A nanotube can be a ballistic conductor with very low resistance, a metallic conductor, or a semiconductor. The nanotubes are also very durable and can withstand multiple crashes while imaging. For example, we have found that a nanotube we mounted to an AFM tip will spring back after being bent back upon itself and still provide good quality images.

We are currently developing expertise in mounting nanotubes to AFM tips using the SEM. Figure 1 shows an AFM image taken with a nanotube attached to the AFM tip using our in-house technique. The image resolution is comparable to an image taken with a commercial AFM tip. Also, in this application, the nanotube provides extended capabilities for high-aspect-ratio probing, tip durability, and electrical conductance.
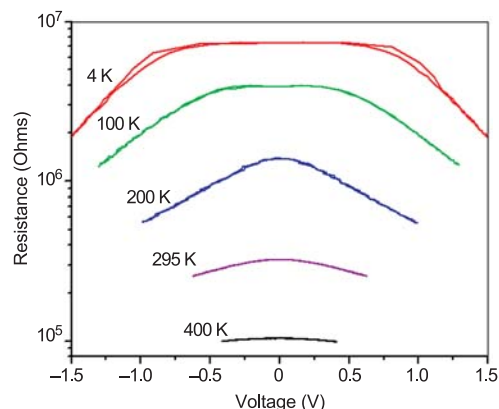
Figure 2: *Resistance versus voltage behavior of a multiwalled nanotube connected to an Au thin-film test structure using electron beam assisted deposition of carbon in the SEM.*

We are also testing the electrical properties of the nanotubes and their subsequent interconnects. Shown in Figure 2 is the resistance versus voltage behavior of a nanotube plus the effects of its interconnects. The resistance response to temperature indicates semiconductive behavior, while the voltage response indicates nonlinear effects possibly due to the interconnects.

Figure 1: *The image above shows a topographic atomic force microscope image of sputter deposited thin-film niobium. The inset is a SEM micrograph of the AFM tip, fabricated at NIST, which took the AFM image. Attached to the end of the AFM tip is the carbon nanotube that actually probed the sample surface. This image demonstrates the resolution and durability of a carbon nanotube as used for AFM imaging.*

Contributors and Collaborators

S.E. Russek (Magnetic Technology Division, NIST); P. Kabos (Radio Frequency Technology Division, NIST); D.S. Finch (Materials Reliability Division, NIST)

Metrology for Nanoscale Properties: Brillouin Light Scattering

A Brillouin-light-scattering facility is being developed for characterizing phonons and magnons at gigahertz frequencies in thin-film materials. The current focus of research is on providing information about the interactions between magnetic modes and thermal phonons, which play a central role in determining the switching times of magnetic-storage devices, spin-valve sensors, and other thin-film magnetic devices.

Ward Johnson and Sudook Kim

Technical Description

Methods that employ Brillouin light scattering (BLS) for the characterization of materials measure the intensity of spectral components of light that is inelastically scattered by acoustic waves (phonons) or spin waves (magnons). Fabry–Perot interferometric techniques are used to acquire accumulated spectra through repeated mechanical sweeping of the etalon spacing.

In this division, research employing BLS is focused primarily on interactions of magnons and phonons in ferromagnetic thin films. This subject is important with respect to maximizing the speed of magnetic-storage devices, spin-valve sensors, and other thin-film magnetic devices because the coupling of spin waves to thermal phonons determines the settling time of the magnetization during a switching event. BLS has the potential of becoming a particularly powerful tool for probing these interactions because it can detect both magnons and phonons at gigahertz frequencies. The aim of our research is to characterize changes in the populations of magnons and phonons induced by ferromagnetic resonant excitation.
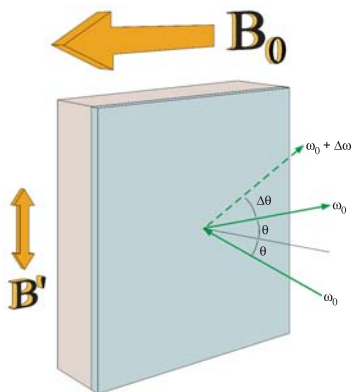
Figure 1: Scattering of light off waves in a thin film in the presence of static and dynamic magnetic fields.

Accomplishments

We have implemented techniques for electromagnetically pumping magnons during BLS measurements. As represented in Figure 1, an oscillating magnetic field B′ at gigahertz frequencies is superimposed on a constant magnetic field B_0 to drive spins into uniform precession (excite magnons with a wavevector of zero). Scattered light undergoes a frequency shift $\Delta\omega$ and a change in direction $\Delta\theta$ relative to the specular reflection, as a result of interactions with acoustic or magnetic waves in the film.
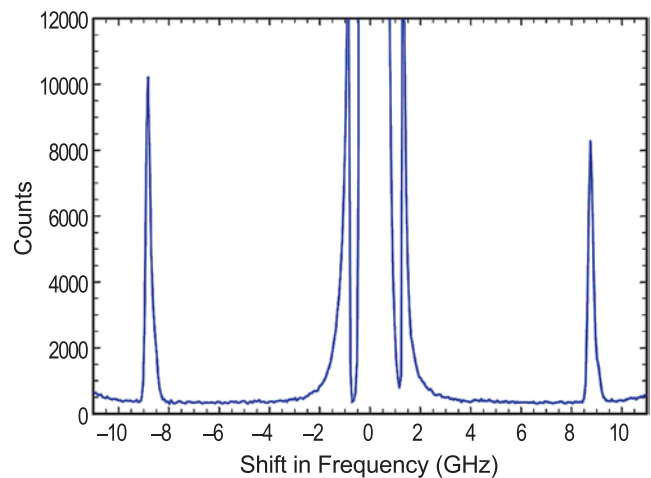
Figure 2: Backscattered BLS spectrum showing 8.8 GHz pumped magnons in a film of $Ni_{81}Fe_{19}$ (0.9 % Tb).

This implementation of magnon pumping in a backscattered configuration enables measurements on opaque films, which cannot be studied using forward-scattering techniques. Ongoing measurements are focused on permalloy ($Ni_{81}Fe_{19}$) thin films doped with Tb, which affects magnetic relaxation. An example of a pumped-magnon spectrum from a 50 nm film of $Ni_{81}Fe_{19}$ (0.9 % Tb) is shown in Figure 2. Counts in the range between –2 GHz and 2 GHz arise from a direct reference beam. Strong magnon peaks appear at the 8.8 GHz pumping frequency.

Contributors and Collaborators

P. Kabos (Radio-Frequency Technology Division, NIST); S. Russek (Magnetic Technology Division, NIST)

The NIST Center for Neutron Research (NCNR)

Growth in nanotechnology requires a means by which the structure and dynamical properties of novel nanoscale materials can be characterized. One of the most effective techniques for this purpose is that of neutron scattering. The NIST Center for Neutron Research (NCNR) provides the nation's scientific community with a broad suite of unique and state-of-the-art neutron measurement capabilities, which are currently used to characterize nanomaterials in many different areas ranging from physics and chemistry, to biology.

J. Michael Rowe and Patrick D. Gallagher

Figure 1: Instruments in the cold neutron guide hall.

The NIST Center for Neutron Research (NCNR) neutron source provides intense beams of neutrons that are used for the characterization of novel nanoscale materials. Neutrons reveal properties of materials that are not available to other probes. They can behave like microscopic magnets, diffract like waves, or set atoms into motion as they recoil from their impact. The wavelengths of the neutrons can be readily varied to cover a range from less than 0.1 nm to 10 nm. Thus neutrons can provide structural information on the nanometer scale. At the same time, the neutrons carry energies of order 1 meV, which is the same order as that of motions of atoms in solids, waves in magnetic materials, or the vibrations in molecules. Because of this fortuitous combination of wavelength and energy, neutrons can provide unique information about the geometry and dynamics of nanoscale objects.

In addition to the thermal energy neutron beams, which emanate from the heavy water or graphite moderators, the NCNR has a large area liquid hydrogen moderator, or cold source, that provides intense neutron beams for the only cold neutron facility presently operating in the United States. There are currently 29 experiment stations located at the NCNR: six provide high neutron flux positions for irradiation, and 23 are beam facilities, most of which are used for neutron scattering research. The figure provided here shows a view of the instruments located within the NCNR guide hall, all of which view the NCNR cold source.

The NCNR supports important NIST research needs, but it also operates as a major national user facility with merit-based access made available to the entire U.S. technological community. Each year, over 1900 research participants from all areas of the country, from industry, academia, and government, use the facility for measurements. Roughly 350 papers are either published or in press each year as a result of the research conducted at the NCNR.

Beam time for research to be published in the open literature is without cost to the user, but full operating costs are recovered for proprietary research. Access is gained mainly through a peer-reviewed, web-based proposal system with beam time allocated by a Program Advisory Committee twice a year. For details, see **www.ncnr.nist.gov/beamtime.html**. The National Science Foundation and NIST co-fund the Center for High Resolution Neutron Scattering (CHRNS) that operates six of the world's most advanced instruments. Time on CHRNS instruments is made available through the proposal system. Some access to beam time for collaborative measurements with the NIST science staff can also be arranged on other instruments.

Pore Size Distributions in Low-κ Dielectric Thin Films from SANS Porosimetry

The microelectronics industry is testing a wide variety of porous low-dielectric constant ("low-κ") materials for future use in integrated circuits. To understand low-κ thin film properties, a quantitative analysis of pore size distribution is vital. The Electronics Materials group has developed a new approach to this challenging problem based on a small angle neutron scattering (SANS) porosimetry technique. The new technique quantifies pore size distribution and reveals subtle material characteristics inaccessible to other measurement techniques.

Barry J. Bauer and Ronald C. Hedden

As feature size on integrated circuits decreases to below 100 nm, electrical crosstalk, or interference between interconnects, becomes a major obstacle to device performance. A need has arisen to develop improved electrical insulating materials for the next generation of microelectronic devices. Silicon dioxide and fluorosilicate glass, the insulators used in today's devices, have dielectric constants (κ) of about 4.2 and 3.7 respectively, but materials with dielectric constants of 2.2 or lower will be needed by 2007. However, it has proven difficult to improve existing materials by changing their chemical structure.

Much of the recent developmental efforts in low-κ dielectrics involve production of nanoporous thin films. By introducing tiny air-filled pores into the material, the bulk dielectric constant is lowered because air has a dielectric constant of 1.0. The microelectronics industry is testing a wide variety of porous low-dielectric constant ("low-κ") materials, including both organosilicate and organic polymer types. To understand the basis for their physical properties, detailed structural characterization is essential. Specifically, quantitative characterization of the pore size distribution is a critical issue because pore size impacts mechanical, thermal, and barrier properties of the films. Because pore size is very small (< 10 nm) and pore volume fraction is high (0.1 to 0.5), microscopy techniques are generally insufficient for evaluation of pore size distribution.

A new approach to pore size determination combines the established science of capillary

porosimetry with a powerful analytical technique, small angle neutron scattering (SANS). Capillary porosimetry is an established experimental technique applicable to determination of pore size distributions. The porous material is exposed to the vapor of a "probe solvent," and pores fill with liquid solvent by capillary condensation. An adsorption isotherm is constructed by measuring solvent uptake as a function of partial pressure. In general, filling of the pores with solvent is size-dependent; the smallest pores fill first as solvent partial pressure is increased. Alternatively, the sample temperature may be varied while solvent partial pressure is held constant. Optical, x-ray, or gravimetric techniques may be employed to measure solvent uptake. Figure 1 shows solvent adsorption curves obtained by specular x-ray reflectivity (SXR) for an organosilicate type low-κ material.

A limitation of capillary porosimetry is that pore size is usually not directly measured but is calculated by applying a physical model to the adsorption data. Serious ambiguities result when hysteresis phenomena are observed, which is normally the case for nanoporous materials. In addition, physical models for adsorption may fail when pores are very small, as in the low-κ dielectrics. Conventional analysis of capillary porosimetry data, therefore, can provide only qualitative comparisons between low-κ materials, not quantitative pore size distributions. However, a great improvement to the technique is possible by using small angle neutron
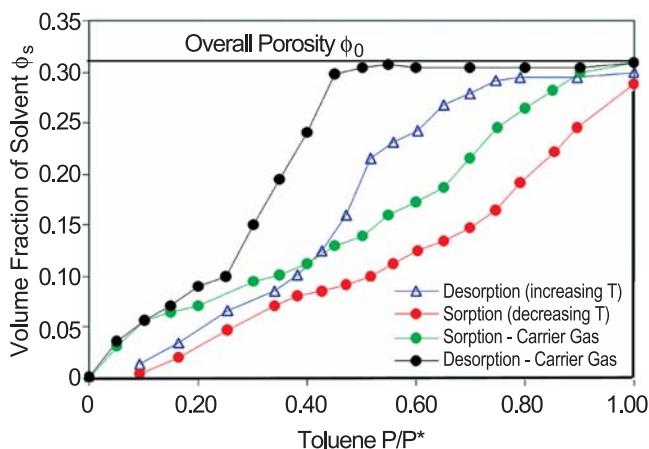
Figure 1: *Solvent adsorption data for an organosilicate low-κ dielectric measured by x-ray reflectivity. Porosimetry is conducted by two methods: under isothermal conditions while varying solvent partial pressure in a carrier gas (green, black), or in a saturated solvent atmosphere while varying sample temperature (red, blue).*

scattering (SANS) to observe the adsorption process. By monitoring the pore filling and unfilling with SANS, important characteristics of the pore size distribution can be quantified irrespective of hysteresis phenomena.

To facilitate SANS porosimetry experiments, a programmable atmospheric control device was constructed that uses mass flow controllers to deliver solvent vapor in air to a flow-through sample cell. The partial pressure P of the solvent can be varied from 0.0 (pure air) to $P*$ (saturated solvent vapor). The sample may also be exposed to solvent vapor at a constant partial pressure P while sample temperature is varied, effectively changing P*.

The first stage of neutron porosimetry is a "contrast match point" determination. The pores are filled with solvent mixtures of variable neutron scattering length density (SLD). The solvent SLD is varied by mixing hydrogen- and deuterium-containing analogs of the solvent. The scattered intensity $I(q)$ from the solvent-filled, porous material depends on the difference in SLD or "contrast" between the solvent and the matrix. The solvent SLD is varied systematically, and the scattered intensity $I(q)$ is measured at each composition. If the material is homogeneous in atomic composition and all of the pores fill with solvent, a contrast match solvent composition exists for which $I(q)$ becomes zero over all q. If the material has inhomogeneities in its atomic composition, or if some of the pores are not filled by solvent ("closed pores"), a contrast match point will not be observed. SANS porosimetry is more applicable to samples with a true contrast match point, as subsequent data analysis is complicated by inhomogeneities.

The second stage of the measurements is porosimetry using solvent vapor of the contrast match composition. SANS data are collected as the partial pressure of the probe solvent is increased (sorption) and decreased (desorption). When pores fill with the contrast match liquid, their SLD matches the sample matrix, so the SANS measurement yields the size of only the "empty" pores. Thus, as solvent partial pressure is increased, pore size is measured for sub-populations of pores of increasingly large size.

If the volume fraction of the solvent in the film is also measured as a function of partial pressure, then average pore size and pore volume fraction are simultaneously known. X-ray reflectivity porosimetry allows such measurement with high precision and is a powerful complement to SANS porosimetry. Figure 2 shows combined results from both techniques: pore size from SANS is plotted *vs.* empty pore volume fraction from SXR. The data are essentially

unaffected by hysteresis phenomena within the limits of uncertainty of the experiment. When all pores are empty, the SANS measurement gives the average pore size for the entire distribution. As pores are filled, the upper end of the pore size distribution is probed because only the larger pores are empty and contribute to $I(q)$ from SANS. For the sample shown in Figure 2, the average pore size is about 60 Å, but the sample contains some pores of 80 Å or larger. By using capillary porosimetry to isolate the scattering from the largest pores, sub-populations of large pores within a low-κ material can be readily identified, provided their concentration is high enough to make a measurable change in the scattering. Such information is valuable to the low-κ integration effort because large pores are a leading cause of device failure.
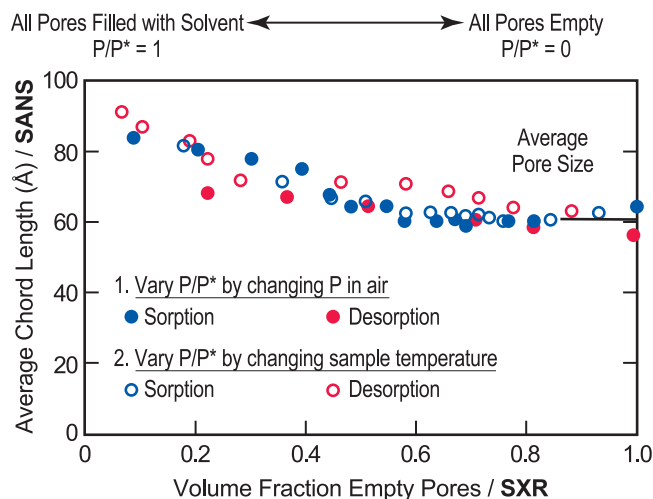
Figure 2: Size information (average chord length) from SANS porosimetry plotted vs. volume fraction empty pores from x-ray reflectivity. The scattering data contain size information related to the average size of only the empty portion of the pores. As solvent partial pressure is increased from P/P*= 0.0 to P/P*= 1.0 (saturated solvent vapor), pores fill with liquid solvent in order from smallest to largest. As P/P* approaches 1.0, the scattering from the largest pores is probed.

The SANS porosimetry technique allows characterization of pore size distribution without a need for a physical model for adsorption. SANS porosimetry is perhaps the most quantitative technique available today for characterizing pore size distribution in nanoporous low-κ thin films.

For More Information on this Topic

B. Bauer, H. Lee (Polymers Division, NIST); R. Hedden (Department of Materials Science and Engineering, The Pennsylvania State University)

Advanced Metallizations for Sub-100 nm Electronics

Electrodeposited copper is rapidly replacing aluminum for on-chip "wiring" because of its lower electrical resistivity, superior electromigration behavior, and the ability to fill fine features without the formation of seams or voids. As feature dimensions go below 100 nm, difficulties in maintaining performance are anticipated. We are addressing these issues through a combination of modeling and experimental efforts. In FY2003, we have pushed the quantitative limits of the Curvature Enhanced Accelerator Coverage (CEAC) mechanism developed in the Metallurgy Division of NIST. Exploration of the mechanism has yielded new electrochemical processing routes for improved metallization and is guiding the development of advanced metallizations beyond copper as well as new processing routes such as ruthenium barriers for seedless electrodeposition of copper.

Thomas P. Moffat and Daniel Josell

This project is meeting the microelectronics industry's need for improved device metallizations by exploring advanced materials and process models for superconformal film growth. In FY2003 we have:

- Developed a two-step process for obtaining superfill during silver electrodeposition;

- Demonstrated superconformal feature filling using ruthenium barriers without copper seeds;

- Described an exact solution for feature filling under conditions of fixed total catalyst coverage;

- Extended the CEAC mechanism to explain surface stabilization of planar deposits during deposition of metals in electrolytes containing surfactant additives;

- Quantified consumption of adsorbed catalyst (neglected in previous CEAC models) which can substantially affect feature filling under certain deposition conditions.

Technical Details

Filling of trenches and vias with silver and copper is quantitatively explained by the Curvature Enhanced Accelerator Coverage Mechanism (CEAC) developed at NIST. Our current measurement and modeling effort is focused on copper and silver metallizations, the latter metal having the lowest resistivity of any element and, thus, having potential on-chip applications.

A two-step process for superfill of high aspect ratio features during silver deposition was demonstrated

for the first time. In this process, the catalyst is adsorbed on the patterned wafer prior to metal deposition; in traditional copper processing, a single electrolyte contains both the catalyst and the metal ions. As explained by the CEAC mechanism, this process offers the possibility of improved filling of finer features with higher aspect ratios through minimization of the conformal "incubation" period of growth. In addition, the plating bath requires fewer components and is thus easier to maintain under industrial conditions.

In a review of NIST research by International Sematech in November 2000, Aaron Frank, Program Manager for Copper Deposition, requested that we also examine a growing problem for on-chip interconnects: poor deposition of seed layers as features shrink. In response to this request, we demonstrated in FY 2003 that superconformal electrodeposition directly on ruthenium barrier layers on *patterned* substrates eliminates the difficulties associated with sputter-depositing copper seeds on tantalum and titanium nitride barriers, again allowing filling of finer features with higher aspect ratios (See Figure 1).

60 nm
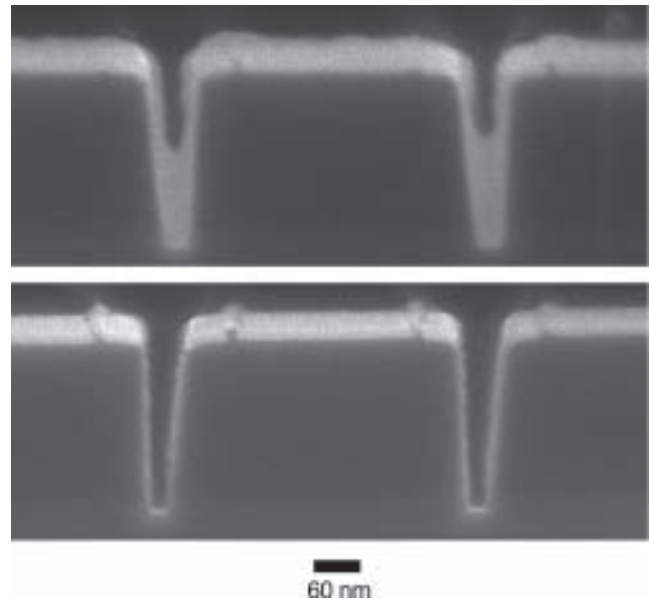
Figure 1: Bottom-up copper fill during electrodeposition in 50 nm wide trenches with no copper seed is visible in the top image. The patterned dielectric with the ruthenium barrier alone is visible in the bottom image.

Computer codes, that quantitatively predict superconformal deposition in fine features through the CEAC mechanism, evaluate concentration fields in the electrolyte as well as surface coverage of adsorbed catalyst on a moving boundary. Our closed-form solution for fixed initial coverage of catalyst can be used to assess the accuracy of these codes, increasing the reliability of

their predictions when applied to more complex conditions including catalyst accumulation and consumption.

In a development with application far beyond the microelectronics industry, our recent publication on the CEAC mechanism of brightening is the first to quantitatively explain the impact of adsorbed catalyst on surface stabilization during growth. This work is possibly the most significant advance in understanding surface stabilization since the growth of surface perturbations due to concentration gradients was first described. It is as significant to creating shiny electrodeposits of metal on a car bumper as it is to reducing defect-inducing surface roughness in feature filling for microelectronics.
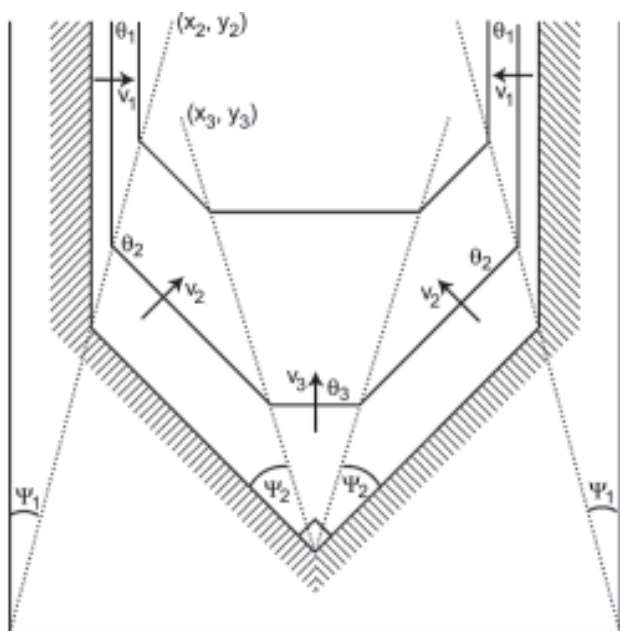
Figure 2: *The geometry used to define the exact solution for the superconformal filling of a trench. The metal deposits at the bottom corners of the trench have met in the middle where a new, even more rapidly moving, growth front emanates.*

Electrochemical and surface analytical measurements on planar substrates were used in FY2003 to establish rates of catalyst consumption that affect both feature filling and, quite likely, the microstructure of the metal deposits. Previous CEAC-based models have discounted such consumption, and this work demonstrates the reasonableness of such assumptions for the previously studied conditions. It also extends the understanding of CEAC mechanism operation to the less than ideal deposition conditions for which catalyst consumption is significant.

Selected Project Publications for FY2003

D. Josell, T.P. Moffat, and D. Wheeler. "An Exact, Algebraic Solution for the Incubation Period of Superfill," *J. Electrochem. Soc.*, *(in press)*.

D. Josell, D. Wheeler, C. Witt, and T.P. Moffat. "Seedless Superfill: Copper Electrodeposition in Trenches with Ruthenium Barriers." *Electrical and Solid-State Letters*, *(in press)*.

G.B. McFadden, S.R. Coriell, T.P. Moffat, D. Josell, D. Wheeler, W. Schwarzacher, and J. Mallett. "A Mechanism for Brightening: Linear Stability Analysis of the Curvature Enhanced Accelerator Coverage Model." *J. Electrochem. Soc.*, *(in press)*.

D. Josell, S. Kim, D. Wheeler, T.P. Moffat, and S.G. Pyo. "Interconnect Fabrication by Superconformal Iodine-Catalyzed Chemical Vapor Deposition of Copper." *J. Electrochem. Soc.*, **150** (5), C368–C373 (2003).

D. Wheeler, D. Josell, and T.P. Moffat. "Modeling Superconformal Electrodeposition Using the Level Set Method." *J. Electrochem. Soc.*, **150** (5), C302–C310 (2003).

B.C. Baker, C. Witt, D. Wheeler, D. Josell, and T.P. Moffat. "Superconformal Silver Deposition Using KSeCN Derivitized Substrates." *Electrochemical and Solid-State Letters*, **6** (5), C67–C69 (2003).

T.P. Moffat, B. Baker, D. Wheeler, and D. Josell. "Accelerator Aging Effects During Copper Electrodeposition." *Electrochemical and Solid-State Letters*, **6** (4), C59–C62 (2003).

S.G. Pyo, S. Kim, D. Wheeler, T.P. Moffat, and D. Josell. "Seam-Free Fabrication of Sub-Micrometer Copper Interconnects by Iodine-Catalyzed Chemical Vapor Deposition." *J. Appl. Phys.*, **93** (2), 1257–1261 (2003).

B.C. Baker, M. Freeman, B. Melnick, D. Wheeler, D. Josell, and T.P. Moffat. "Superconformal Electrodeposition of Silver from a KAg(CN)$_2$-KCN-KSeCN Electrolyte." *J. Electrochem. Soc.*, **150** (2), C61–C66 (2003).

T.P. Moffat, D. Wheeler, C. Witt, and D. Josell. "Superconformal Electrodeposition Using Derivitized Substrates." *Electrochemical and Solid-State Letters*, **5** (12), C110–C112 (2002).

D. Josell, B. Baker, C. Witt, D. Wheeler, and T.P. Moffat. "Via Filling by Electrodeposition: Superconformal Silver and Copper and Conformal Nickel." *J. Electrochem. Soc.*, **149** (12), C637–C641 (2002).

Our findings have also been conveyed to the U.S. microelectronics industry, academia, and other national laboratories through more than 15 external presentations in the last year, including an invited presentation at Intel's Portland, Oregon facility. Project publications generated 100+ citations in the past year.

For More Information on this Topic

D. Josell, D. Wheeler, T.P. Moffat (Metallurgy Division, NIST)

Modeling Dynamics, Damping and Defects for Perpendicular Magnetic Recording Media

In its accelerating march toward ever higher recording densities, the hard disk drive industry is moving toward perpendicular recording, where the magnetization of the written bits is directed perpendicular to the disk surface. One of the metrology needs generated by the shift to perpendicular recording is the characterization of inhomogeneity in the media. This article describes our development of models that enable measurement of inhomogeneity in perpendicular media by ferromagnetic resonance.

Robert D. McMichael

One of the growing metrology needs of the hard drive industry is the ability to characterize the new generation of perpendicular recording media, where the information is stored as magnetic bits magnetized perpendicular to the disk surface. To store these bits, it is desirable to have media with small, nearly decoupled grains with strong, uniform anisotropy and easy axes directed along the disk normal. Typical grain sizes in the new media are approximately 10 nm.

Characterization of the average properties of perpendicular media is routinely accomplished by magnetometry. However, there is a significant need for information about the inhomogeneity of perpendicular media, particularly the angular easy axis distribution and the distribution of anisotropy fields. Inhomogeneity of the media impacts the bit writing process, analysis of bit stability, and media noise in the read process.

Information about the dispersion of the crystallographic axes can be obtained from x-ray diffraction, but magnetic coupling may force two crystallographically distinct grains to behave as a single magnetic grain, so a purely magnetic measurement of the dispersion angle would be more closely related to the performance of the media.

For variations in the anisotropy field, the only estimates currently available are based on TEM compositional analysis coupled with anisotropy studies on bulk materials. Here again, a direct, purely magnetic measurement would give a clearer indication of the magnetic performance of the media.

The new perpendicular media, with aligned anisotropy axes, is much better suited to ferromagnetic resonance measurements than longitudinal media. Ferromagnetic resonance is a peak in the transverse susceptibility at a frequency that corresponds to precession of the magnetization about its equilibrium orientation. The width of the ferromagnetic resonance peak, or "line width," is the combined effect of damping and inhomogeneity. While there are well-established models for damping, better models of inhomogeneity were needed for interpretation of line width data.

Through our modeling the dynamics of inhomogeneous films, we have laid the theoretical support needed for interpretation of line width data to obtain inhomogeneity information on magnetic thin films.

Previously, there were two known models of ferromagnetic resonance line broadening by inhomogeneity: the "local resonance" model and the "two-magnon" model. The local resonance model assumes that interactions are not important, and the line width is therefore a direct measure of the inhomogeneity strength. The "two-magnon" model includes interactions but, because it is a result of perturbation theory, is limited to weak inhomogeneity. The two-magnon linewidth depends quadratically on the inhomogeneity strength. The models give very different results, but both models have been successfully used to describe separate sets of linewidth data.
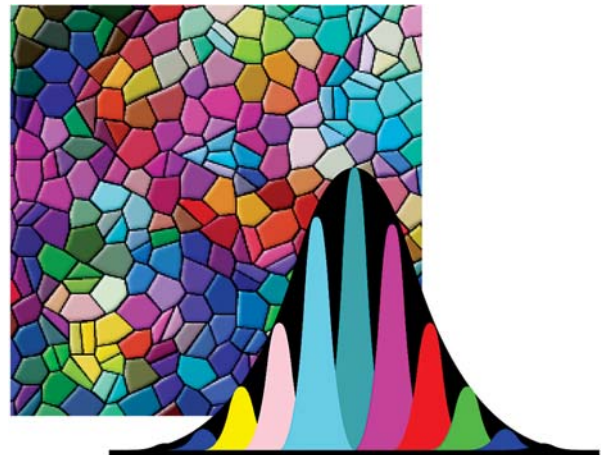
Figure 1: *In the absence of interactions, inhomogeneity leads to local resonances at a distribution of frequencies, leading to a broadened resonance line. Interactions cause narrowing of the envelope peak described by the two-magnon model.*

To understand the relationship between the local resonance and two-magnon models of line width, we modeled a series of inhomogeneous films with different grain sizes and different levels of inhomogeneity, and we computed the eigenmodes of the magnetization

motion (Figure 1). We found that the behavior of the magnetization dynamics depends on the relative strengths of the interactions and the inhomogeneity. For a uniform film, the eigenmodes are spin waves ("magnons" in quantum mechanics), and inhomogeneities or strong interactions cause mixing of the spin wave modes in agreement with the two magnon model. For strong inhomogeneities relative to interactions, the dynamics were localized on individual grains in agreement with the local resonance model. These results are summarized in Figure 2, where small grain sizes correspond to strong intergranular interactions, and large grains correspond to weak interactions. These results unify the local resonance and two-magnon models.
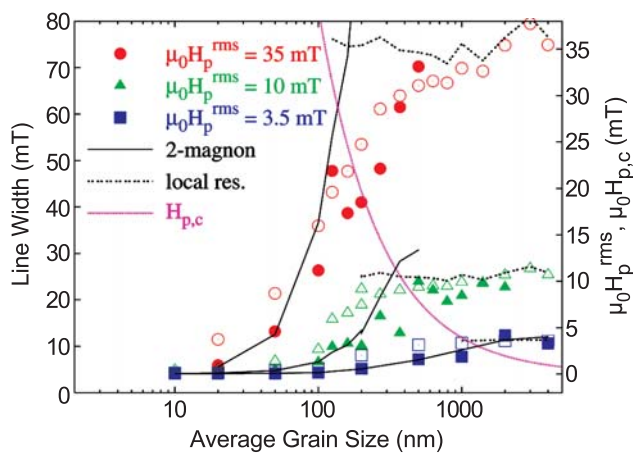
Figure 2: *Line widths as a function of grain size in a Permalloy film calculated by eigenmode analysis for three random field strengths H_p. (Open and closed symbols are for two methods of computing line width from the eigenmode spectrum.) The line width transitions smoothly from the local resonance model for large grains (weak interactions) to the two-magnon model when grains are small. The pink line indicates where interactions and inhomogeneity are roughly equal.*

The full eigenmode analysis takes a significant amount of computation time, making it a poorly suited technique for data fitting. However, the results in Figure 2 suggest a simple first approximation; for a given combination of microstructure and inhomogeneity, the lesser of the two-magnon model and the local resonance model is likely to be valid, except in the range where they are similar.

Figures 3 and 4 show two-magnon and local resonance line width calculations for perpendicular media with thickness 15 nm and grain size 10 nm with an average anisotropy field of 1.4 T (14 kOe). In these figures, the top diagram portrays the local resonance result, the green curve is the two-magnon model with dipolar interactions only, and the blue and pink curves are for fractional and full exchange coupling. For the given inhomogeneity strengths, the two magnon model results are expected to be a good

approximation to the line width, but for larger values of inhomogeneity, the two magnon results will exceed the local resonance values and the local resonance results would be valid.
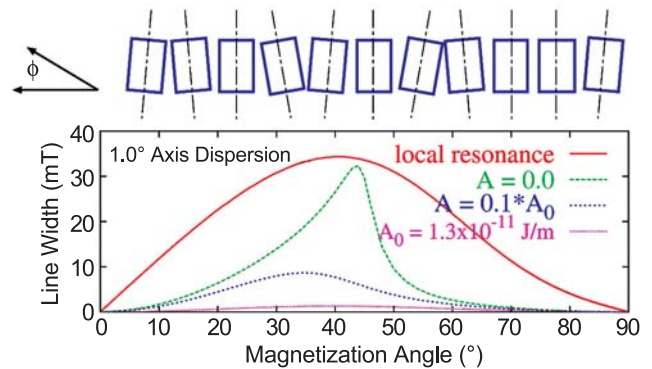
Figure 3: *Local resonance and two-magnon line widths resulting from tilting of the easy axis directions in perpendicular recording media with 10 nm grains. Two magnon results are calculated for three values of exchange coupling.*
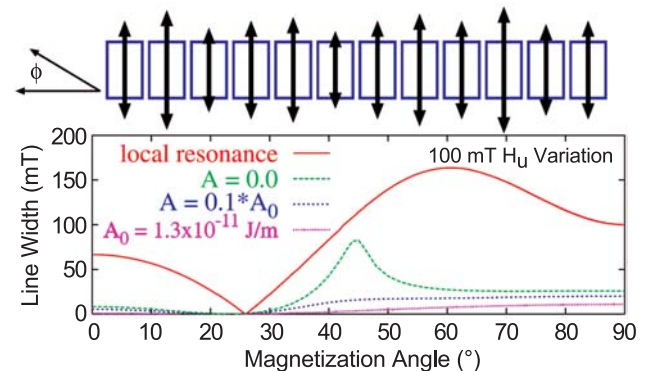
Figure 4: *Local resonance and two-magnon line widths resulting from anisotropy variations in perpendicular recording media with 10 nm grains. Two magnon results are calculated for three values of exchange coupling.*

These results show that the ferromagnetic resonance line width can be a sensitive probe of inhomogeneity in perpendicular recording media with the ability to differentiate damping, c-axis dispersion, and anisotropy variations. For weak inhomogeneity, the two-magnon model becomes valid, and the line width can also provide information about exchange coupling.

A ferromagnetic resonance apparatus with the frequency and field ranges necessary to measure perpendicular media is in the design phase.

For More Information on this Topic

R.D. McMichael, W.F. Egelhoff, Jr. (Metallurgy Division, NIST)

R.D. McMichael, D.J. Twisselmann, A. Kunz, *Phys. Rev. Lett.* **90**, Art. No. 227601 (2003).

Magnetic Properties of Nanostructured Materials

In the past 10 to 15 years, there has been a remarkable improvement in the technology for materials preparation, resulting in today's capability of controlling morphology and features at the nanometer level. In magnetic materials, such control allows the fabrication of nm-thick (or separated) composite materials of dissimilar magnetism, leading to materials with novel magnetic character and unusual property combinations. We provide the understanding and metrology that allows U.S. industry to take advantage of these new materials.

Alexander J. Shapiro and Robert D. Shull

Present day high-density data storage is possible due to the giant magnetoresistance (GMR) spin valve, which is now used as the read head in magnetic disc drives. This structure is composed of two ferromagnetic (FM) layers separated by a thin non-magnetic layer. When an external magnetic field reverses the magnetization of one of the FM layers, the resistance of the composite changes. Consequently, one FM layer must maintain a constant magnetization during this process, usually accomplished by placing an antiferromagnetic (AF) layer adjacent to it so as to "exchange-bias" that FM layer. This results in a hysteresis loop that is shifted along the field axis as shown in Figure 1(a). Unfortunately, this exchange-biasing is not well understood.
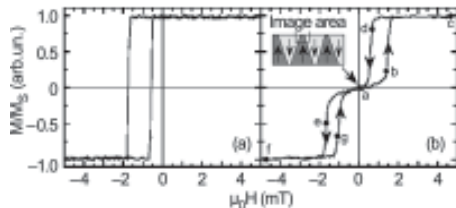
Figure 1: *Hysteresis loops for a NiFe/FeMn bilayer cooled under (a) constant and (b) alternating field conditions.*

Several years ago, we found we could elucidate some of the basics of the magnetization reversal process in such systems [V.I. Nikitenko, *et. al.*, PRB **57**, R8111 (1998)] by using the magneto-optic indicator film technique (MOIF) developed in our laboratory. This domain imaging technique enabled us to show for the first time that, contrary to popular thought, the two sides of the hysteresis loop are not symmetrical but are each governed by different mechanisms. This year, we have answered another key question regarding exchanged bias systems: do the domain walls in the AF move when the FM reverses its magnetization? MOIF observations were made of a NiFe (FM)/FeMn (AF) bilayer which had been ac-demagnetized above the

Neel temperature of the AF but below the Curie point of the FM (Figure 1b). Application of the alternating field at elevated temperatures formed a demagnetized FM composed of striped domains with alternating magnetization vectors, shown in Figures 1(b) and 2(a), on top of coincident AF domains. When a field was applied to this bilayer to saturate the FM [Figures 2(c), (f)], there still remained a remnant image of the original domain pattern (Figure 2a), indicating the AF wall below the FM has not moved.
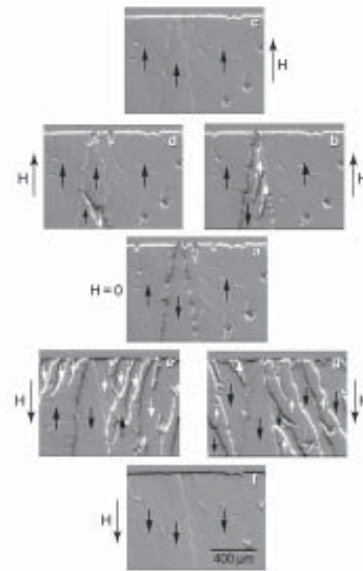
Figure 2: *MOIF images of domains in the FM at the conditions specified by the positions designated in Figure 1(b).*

Some AF spins in the region of the AF/FM interface, however, are changing during the FM reversal, as attested to by the fact that Figures 2(e) and (g) only show domain activity in the same areas for both field application and removal respectively, contrary to that for a normal ferromagnet. Similar observations have also been made on a different AF/FM bilayer, FeMn/$Fe_{76}Mn_6C_{18}$, wherein the initial coincident domain structure in the FM and AF was created by elevated temperature preparation under a low applied field.

As a result of these measurements, theoretical models may now be improved, and industry should now be able to better tailor spin valve processing to obtain improved reproducibility. In the past year, over 40 % of all papers on exchange-biasing have referenced our MOIF results.

Contributors and Collaborators

V. Nikitenko, V. Gornakov (Russian Academy of Sciences); C.L. Chien (Johns Hopkins University); H.-W. Zhao (Chinese Academy of Sciences)

Nanomagnetodynamics

This project provides the magnetic information storage industry with metrology for magnetization damping and magnetic inhomogeneity in thin film ferromagnets. Damping is expected to become a critical issue for magnetic information storage at GHz data rates, and inhomogeneity on the scale of 10 nm in recording media is important for increased storage density in the new generation of disk drives, which will use perpendicular magnetic recording.

Robert D. McMichael

The central issue in interpretation of ferromagnetic resonance line width data is the determination of how much of the ferromagnetic resonance line width is due to damping and how much is due to inhomogeneity. Ferromagnetic resonance is observed as a peak in the transverse susceptibility that occurs when the frequency of the driving field is close to the frequency of precession. The peak position can be used to determine sample average properties, but the width of the resonance peak, or "line width," is a combined effect of damping and inhomogeneity.

Existing simple models describe the contribution of damping to the line width. We have provided reliable models of inhomogeneity that are key to interpretation of line width data. These models describe the line
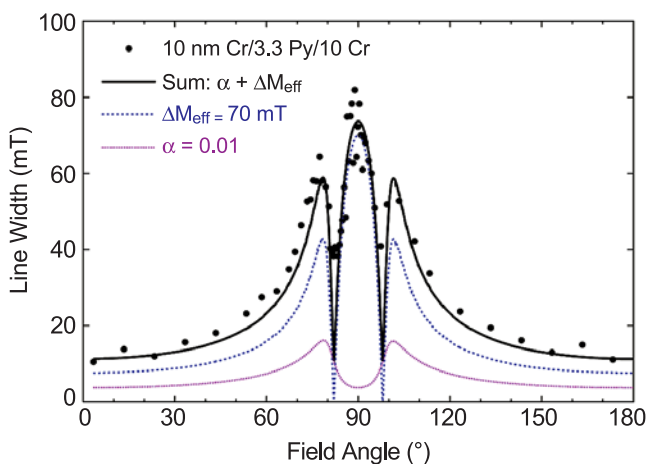
Figure 1: Ferromagnetic resonance linewidth for a Cr/Permalloy/Cr trilayer as a function of applied field angle. This plot illustrates the ability to separate the linewidth into a damping component (pink line) and an inhomogeneous component (blue line) corresponding to 7 % variations in the effective magnetization.

width behavior as a function of frequency and applied field orientation for different types of inhomogeneity.

Neglecting the exchange and dipolar interactions that are characteristic of ferromagnets, local variations in magnetic properties would be expected to result in a distribution of local precession frequencies and a broadened resonance peak. However, interactions tend to synchronize the precession in neighboring regions, effectively "smoothing" the inhomogeneity, and reducing its effect on the line width.

Significant accomplishments in FY03 include:

- Development of a unified model of inhomogeneous line broadening in thin films. This model covers the full range of inhomogeneity and interaction strengths but is computationally too expensive to use for fitting. This model established that the transition from local to collective behavior is governed by the relative magnitudes of the inhomogeneity and the region-to-region coupling. See R.D. McMichael, D.J. Twisselmann, and Andrew Kunz, *Phys. Rev. Lett.,* **90,** Art. No. 277601 (2003).

- An approximation to the full calculation of inhomogeneous line broadening using the "two magnon" model in the strong coupling/weak inhomogeneity limit and local resonances in the weak coupling/strong inhomogeneity limit.

- Useful analytical approximations for the "two magnon" model for ultra thin films in the limit of zero damping.

- Measurement of the damping properties of Cr in proximity to Permalloy (Figure 1). These experiments imply that ferromagnetic resonance measurements in CoCr based hard drive recording media will not be hindered by excessive damping.

- Modeling of ferromagnetic resonance line widths in perpendicular recording media under development in industry.

Contributors and Collaborators

D.J. Twisselmann, W.F. Egelhoff, Jr., A.P. Chen (Metallurgy Division, NIST); Andrew Kunz (Lawrence University); H. Nakamura, M.E. McHenry (CMU); S. Rezende (Recife, Brazil); G.S.D. Beach, A.E. Berkowitz (UCSD)

Anomalously Large Low Temperature Intermixing in Metallic Thin Films

The objective of this program is to provide assistance to U.S. companies in the ultra-high density data storage industry, which includes such products as hard disk drives and magneto-resistive random access memory chips. Our work provides U.S. companies with significant competitive help by investigating the scientific issues underlying the manufacturing process. Often, this scientific understanding will point the way to improved manufacturing processes.

William F. Egelhoff, Jr.

As the scale of microelectronic devices shrinks, surfaces and interfaces play increasingly important roles as they become a larger fraction of the total device volume. Interfaces are especially important for the metallic thin films so common in layered device structures. Interfaces between thin films may appear to be abrupt at macroscopic length scales but diffuse at atomic length scales. Fortunately, when metallic thin films are deposited on one another at room temperature, there is generally little intermixing at the interface. Typically, if there is any intermixing, it is limited to one or two atomic layers. However, recent collaborative studies by NIST and the University of Durham have shown that such low-temperature intermixing can be far more extensive when Al and a transition metal (TM) are involved.

Thin film samples of the type "Al on TM" and "TM on Al" were prepared at the NIST Magnetic Engineering Research Facility and analyzed by grazing-incidence x-ray reflectometry (GIXR) at Durham. GIXR is an ideal technique for these studies since it is extremely sensitive to intermixing at interfaces. We find the intermixing profile perpendicular to the interface is usually well described by a Gaussian distribution, as expected, since diffusion processes often follow Fick's Law. The results are displayed in Table 1 as the full-width-at-half-maximum (FWHM) of the intermixed region. The FWHM results span the range from 0.1 nm for Al on W to 16.8 nm for Cu on Al. This Cu-on-Al result corresponds to approximately 100 atomic layers of intermixing. Such results are a great surprise to researchers in the field. For example, electronic properties for a thin film structure consisting of 2 nm Cu / 1 nm Al / 2 nm Cu were recently reported and analyzed as if the interfaces were atomically sharp. In fact, the sample must have been essentially a random alloy!

Among other combinations showing large intermixing were Mn on Al with 15.1 nm and V on Al with 9.4 nm. These surprising results suggest that the heat of alloying is driving much more extensive chemical reactions at the interface than had heretofore been known. These results have important implications for many microelectronic devices incorporating Al films. For example, problems in magnetic-tunnel-junction devices may be directly attributed to such phenomena. NIST is also developing solutions to such problems based on oxide barriers to suppress the intermixing.

Table 1: **The intermixing FWHM (in nanometers) for thin films of Al on transition metals and transition metals on Al**

TM Element	Al on TM	TM on Al
Ti	1.7	5.0
V	2.6	9.4
Cr	0.5	3.3
Mn	10.4	15.1
Fe	0.9	2.1
Co	0.8	6.8
Ni	1.4	7.9
Cu	2.8	16.8
Zr	1.0	5.1
Nb	0.8	3.6
Mo	1.3	3.4
Ru	0.8	5.2
Rh	0.4	4.7
Pd	4.8	5.6
Ag	2.5	4.5
Hf	2.0	4.4
Ta	0.1	0.9
W	0.1	3.5
Re	2.1	8.6
Os	0.1	7.1
Ir	0.2	5.4
Pt	1.9	4.5
Au	5.2	6.3

Contributors and Collaborators

Detecting Magnetic Nano-Twists in Hard-Disk Reading Heads Using Polarized Neutron Scattering

The nanoscale magnetic films in magnetic reading heads have multiple magnetically active layers. Some of these layers track the varying magnetization of the storage medium, and others stay constant, thus providing a known reference layer. It is anticipated that some of these mobile layers change their magnetization by producing a magnetic twist. Confirming this behavior is difficult using conventional techniques. We have developed a technique which greatly simplifies this metrological challenge.

Kevin V. O'Donovan and Julie A. Borchers

The magnetic recording industry has been steadily increasing the density of storage in computer hard disks. Reading the stored data depends critically on the well-characterized and predictable behavior of nanoscale magnetic films in the reading head. It is thought that some of the layers which track the data change their magnetization by producing a magnetic twist.

NIST researchers working at the NIST Center for Neutron Research have developed an extension of polarized neutron reflectometry (PNR) to enhance its sensitivity to buried magnetic twists. Techniques other than PNR typically measure only the average orientation of the magnetic spins. Earlier techniques of measuring PNR provide depth sensitivity to most magnetic structures but cannot readily distinguish a twist in these materials from a magnetic structure in which all the layers are aligned. PNR measurements can now exhibit enhanced contrast for magnetic twists by simply measuring the reflectivity from the front and back of the sample. Key features in the data

immediately indicate the presence of a twist, as demonstrated in a collaboration with researchers from IBM.[1,2]
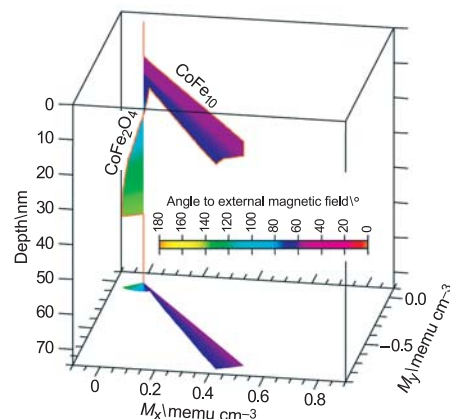
Figure 2: *Magnetic structure derived from fit in Figure 1, as well as its projection into the xy plane. The color coding shows the angle of the magnetization with respect to the applied magnetic field.*

Now a new collaboration with researchers at Hitachi is applying this PNR technique to the basic components of an advanced reading head for hard disk drives. Figure 1 shows the results of the new scattering technique applied to an $CoFe_{10}|CoFe_2O_4$ spin valve. In the absence of a twist, the figure should be nearly symmetrical about the center. However, the strong asymmetry in the spinflip reflectivity at the q's labeled 0.2 nm^{-1} indicates a twisted magnetic structure. The structure fit to the data was determined to be that shown in Figure 2. The twist was expected to be confined to depths colored blue through purple. This new measurement identified an unexpected twist in the depths colored green through powder blue.

References

[1] K.V. O'Donovan, J.A. Borchers, C.F. Majkrzak, O. Hellwig, and E.E. Fullerton. *Physical Review Letters* **88**, 067201 (2002).

[2] K.V. O'Donovan, J.A. Borchers, C.F. Majkrzak, O. Hellwig, and E.E. Fullerton. *Applied Physics A* **74**, S1544 (2002).

[3] K.V. O'Donovan, J.A. Borchers, S. Maat, M.J. Carey, B.A. Gurney. Accepted by *Journal of Applied Physics* (2004).

Contributors and Collaborators

C. Majkrzak (NIST Center for Neutron Research); S. Maat, M. Carey, E. Fullerton, B. Gurney (Hitachi Global Storage Technologies); O. Hellwig (BESSY)

Figure 1: *Polarized neutron reflectivity and fits of a spin valve measured at 47 mT after saturating at –700 mT. The insets show the scattering geometry from each surface*

Nanomanufacturing

In nanoscale manufacturing, knowledge of inherent and process-induced properties is crucial. In new realms of nanoscale manufacturing, nanomaterials will be manufactured in nanoliter volumes, combining so-called top-down and bottom-up or self-assembly approaches. Miniature tools to characterize such materials and processes are needed. We are developing devices that can impose a wide variety of process flows and measure flow-induced properties at transient and persistent conditions.

Steven Hudson and Frederick Phelan, Jr.

The four-roll mill is a macroscopic flow device that has played a critical role in elucidating the interactions between flow and material response. In the microscale regime, an analogous device is needed to efficiently characterize fluids. Merely scaling down the four-roll mill to microscopic dimensions is inherently problematic due to the rotating components. Instead, we are developing a device which uses pressure-generated flow to achieve the same flow types as a four-roll mill, but is miniaturizable, and has greater control over the flow. It is also integrable into high power microscopes and scattering devices.
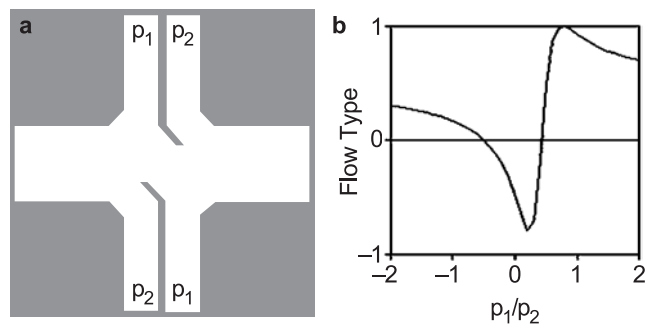
Figure 1: *a) Design of a microchannel analog of the 4-roll mill. b) Flow type as a function of pressure ratio p_1/p_2. Flow type values equal to –1, 0, and 1 correspond to pure rotation, shear and extension, respectively.*

To evaluate various candidate geometries for a pressure-driven microchannel device, flow generated in these devices was calculated in the (Stokes) limit of low Reynolds number by the finite element method. Although a variety of geometries produce highly extensional flow, shear flow is produced at the stagnation point only when opposing channels are offset laterally. A suitable geometry is shown in Figure 1. A wide range of flow type, including pure shear, is possible in this device by adjusting the relative flow rate

in the channels. The relative amount of rotation and its direction can also be adjusted. Figure 2 illustrates the flow streamlines for conditions that yield extensional and shear flow.
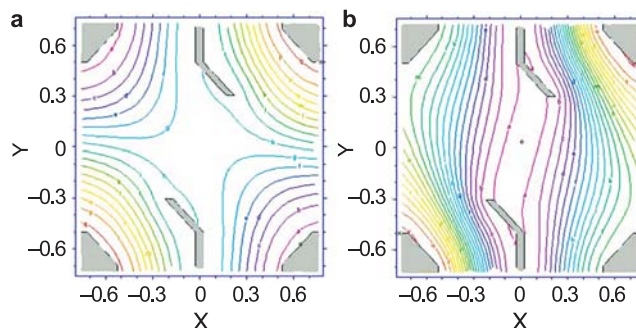
Figure 2: *2D Stokes calculations of pressure-driven flow in microchannels. Streamlines are shown for a) extensional and b) shear flow conditions.*
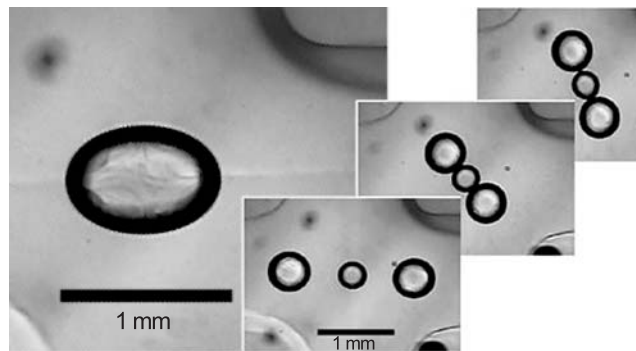
Figure 3: *Images of drops in a computer-controlled cross-channel extensional flow device. Image analysis control feedback adjusts the flow to keep the drop(s) at the stable stagnation point of the device during deformation (shown at left) and collision experiments (series at right).*

A computer control system, with image analysis feedback, has been developed. Experiments with immiscible polymeric fluids have demonstrated that, by using this device, drops can be moved into the device, placed at the stagnation point, deformed, and broken (Figure 3). Drops were then caused to collide and coalesce. Surface tension-driven relaxation of drop deformation has been measured. Based on these results, a focused project to measure interfacial tension, with partner companies in the NIST Combinatorial Methods Center (NCMC), was established.

Contributors and Collaborators

J.T. Cabral, J.A. Pathak (Polymers Division, NIST); NIST Combinatorial Methods Center Focused Project (with member companies) to measure interfacial tension.

Process Monitoring of Polymer Clay Nanocomposites

Real-time, on-line measurements of polymer composite materials properties are desirable not only because they preempt the need for post-processing characterization but also because they can be used to monitor resin conditions, to detect problems with processing parameters, to control the process, and to predict performance of the final product. In this project, we have developed measurement techniques based on optical, dielectric, and rheological techniques. NIST has filled an industry need by designing and constructing process sensors and by collaborating with industry partners in the application of new sensor technology to process monitoring.

Anthony J. Bur

The state of microstructure that forms during the compounding of polymer and clay nanocomposites determines their performance properties. On-line, real-time measurements that are sensitive to microstructure conformation yield a database that can improve efficiency and productivity by giving processors immediate knowledge of the microstructure state. Real-time measurements can potentially minimize the extent of off-line microstructure determinations using x-ray and Transmission Electron Microscopy (TEM) observations. The on-line instrumentation that we have developed is a multifunctional device that contains dielectric, pressure, optical, and ultrasonics sensor ports. The instrument is designed to attach to the end of a twin-screw extruder. The resin flow through the sensor conforms to a slit that is 2 mm high by 28 mm wide, and the sensors are aligned to interrogate the resin in the slit region. The extrudate, shown in the picture below, consists of a strip of material that can be cut into pieces for off-line measurements.

Optical Sensor

Dielectric Sensor

Dielectric Slit Die Housing

Polymer/Clay Nanocomposite
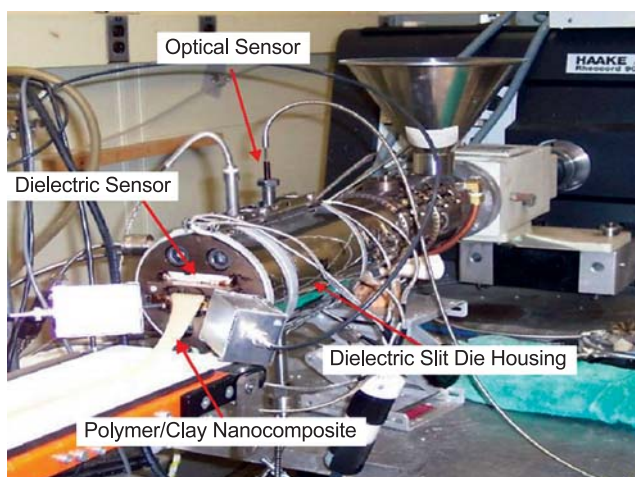
Nylon 6, when compounded with certain clays containing polar organo modifiers, can form a nanocomposite consisting of exfoliated silicate platelets that are a few nanometers thick by tens of nanometers in diameter. On the other hand, if the organo modifier is nonpolar, then the clay particle remains in its aggregate condition of a micrometer size particulate when compounded with nylon 6. When the composite is subjected to an alternating electric field, the dielectric contrast between particle and resin forms a resistance–capacitance network that expresses a dielectric relaxation known as a Maxwell–Wagner (MW) relaxation. The characteristic relaxation time of the resin/nano-platelete combination is longer than that of the resin/aggregate because the nanosize silicate platelet has a high, effective capacitance.

The table shows characteristic relaxation times and dielectric relaxation strengths $\Delta\varepsilon$ for three compounded nylons: neat, exfoliated clay nanocomposite, and aggregate clay composite. The measurements were carried out at processing temperature, 240 ºC. After correcting the data for DC conductivity and electrode polarization effects, we observed only one dielectric relaxation in the neat polymer, but two relaxations were observed in the composites. The single relaxation of the neat is associated with the α relaxation (log f = 2.40) of the macromolecule, and the two relaxations of the composites are the α relaxation (log f = 2.70 and 2.46) and the MW relaxation at log f = 1.98 and 1.33 for which the exfoliated microstructure displays the lowest characteristic frequency. Large $\Delta\varepsilon$ is characteristic of MW relaxation.

	NY 6 neat	NY 6/clay aggregate	NY 6/clay exfoliated
Log f_1	2.40	2.70	2.46
Log f_2		1.98	1.33
$\Delta\varepsilon_1$	441	1700	2200
$\Delta\varepsilon_2$		18,200	18,400

Contributors and Collaborators

Electrochemical Processing of Nanoscale Materials

Precise temporal control of supersaturation provided by electrochemical methods holds promise for the synthesis and characterization of materials and structures of very small dimensions — nanomaterials. Variation of the electrochemical potential leads not only to changes in the metal deposition rate but also effects the adsorption of surfactants and segregation phenomena which exert a strong influence on the morphological evolution and stability.

Thomas P. Moffat and Jon Mallett

Electrochemical synthesis has become an important tool in the fabrication of nanoscale devices and structures. Modulation of the electrode potential can be used to create films with a corresponding variation in composition and/or structure. This allows materials, such as multilayers and nanocontacts, to be engineered with submonolayer precision. Likewise, knowledge of the stability and reliability of these finite size structures will be central to any technical application.

In the last year, we have continued using scanning probe microscopy to characterize the structure and stability of immersed surfaces. This work ranges from atomically resolved STM studies of adsorbate dynamics to AFM measurements of roughness evolution during electrodeposition. The focus of this activity is strengthening our knowledge of the connection between atomistic processes and morphological evolution observed at larger length scales.

A new aspect of our program this year is the study of nanocontacts formed by electrodeposition between two electrodes. Physical property measurements of these junctions have revealed a variety of effects such as quantized conductance, ballastic magnetoresistance,
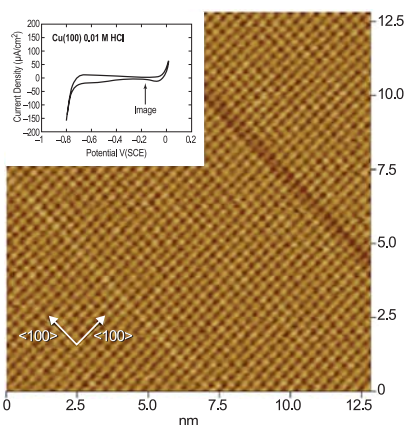
Figure 1: A high resolution STM image of a c(2x2) chloride adlayer on Cu(100) in 0.01 mol/L HCl. The image was collected at –0.150 V SCE as shown on the inset voltammogram.
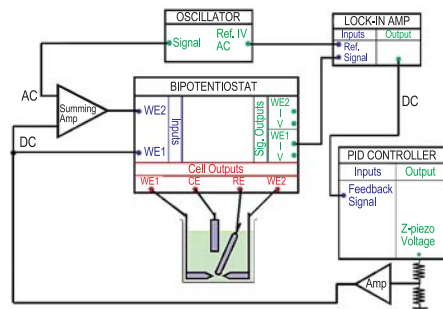
Figure 2: Schematic of control circuit used for forming and maintaining contacts of fixed conductance.

and adsorbate-influenced surface scattering. Many investigations use electrodeposited contacts, yet limited techniques are available for growing and maintaining such junctions at a fixed or predetermined conductance. At NIST, we have combined a bipotentiostat with a STM-like feedback circuit in order to form electrodeposited metal contacts of predetermined fixed resistance.
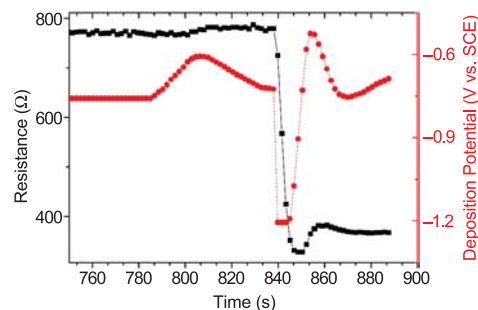
Figure 3: Controlled step in nanocontact resistance.

The junction conductance measured with a lock-in-amplifier is compared with a preset value, and the electrochemical potential of the two working electrodes is adjusted to either deposit or etch material to obtain the specified conductance value. Figure 3 shows a controlled transition in contact resistance between 778 Ω and 369 Ω. Careful choice of the feedback control parameters resulted in transients with only one damped oscillation. Stable contacts have been grown between 800 Ω and 2 Ω.

In the coming year, the measurements outlined above will be extended towards problems relevant to micro- and molecular electronics.

Contributors and Collaborators

W.F. Egelhoff, H. Ettedgui, E.B. Svedberg, J.E. Bonevich, R.D. McMichael (Metallurgy Division, NIST)

Organizational Charts

Materials Science and Engineering Laboratory

L.E. Smith, Director
S.W. Freiman, Deputy Director

Metallurgy
C.A. Handwerker, Chief
F.W. Gayle, Deputy

Polymers
E.J. Amis, Chief
C.R. Snyder, Deputy

Ceramics
D.L. Kaiser, Chief
D.R. Black, Deputy

Materials Reliability
A.F. Clark, Chief
T.A. Siewert, Deputy

NIST Center for Neutron Research
J.M. Rowe, Director
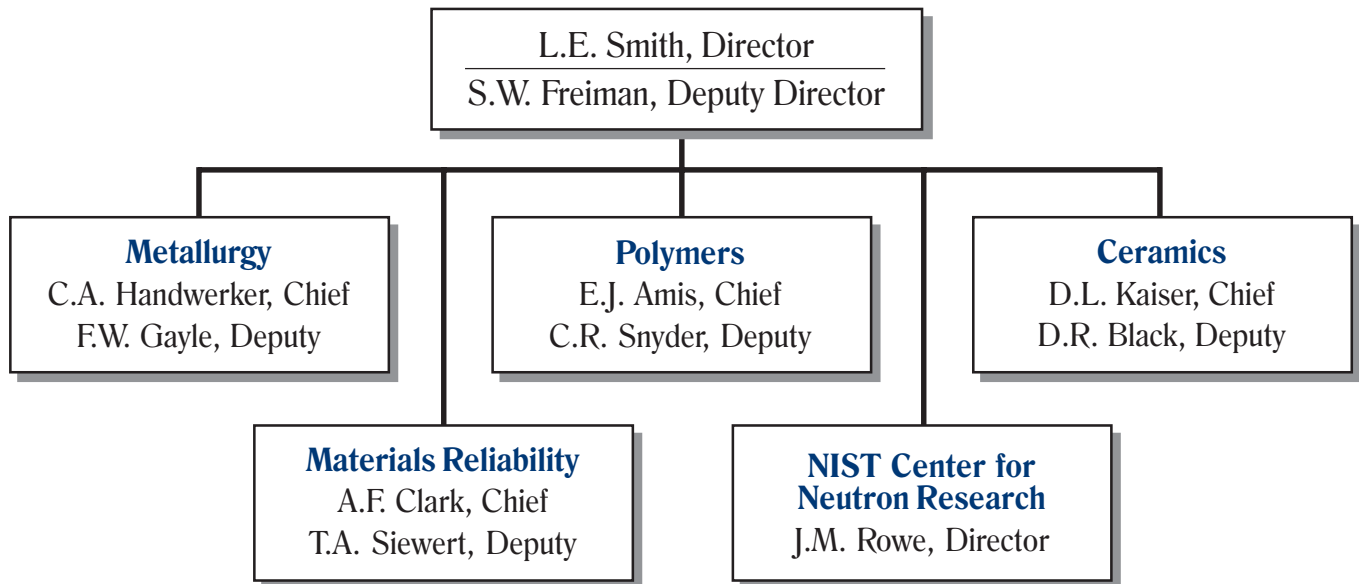
National Institute of Standards and Technology

Director
Boulder Laboratories

Director
Deputy Director

Baldrige National Quality Program

Director for Administration & Chief Financial Officer

Technology Services

Advanced Technology Program

Manufacturing Extension Partnership

Manufacturing Engineering Laboratory

Chemical Science and Technology Laboratory

Materials Science and Engineering Laboratory

Electronics and Electrical Engineering Laboratory

Information Technology Laboratory

Physics Laboratory

Building and Fire Research Laboratory